01 Sep 2012

A New Model for the Spectral Induced Polarization Signature of Bacterial Growth in Porous Media

Andre Revil

Estella A. Atekwana
Missouri University of Science and Technology, atekwana@mst.edu

C. Zhang

Abderrahim Jardani

et. al. For a complete list of authors, see https://scholarsmine.mst.edu/geosci_geo_peteng_facwork/1305

Recommended Citation

A. Revil et al., "A New Model for the Spectral Induced Polarization Signature of Bacterial Growth in Porous Media," *Water Resources Research*, vol. 48, no. 9, American Geophysical Union (AGU), Sep 2012.
The definitive version is available at https://doi.org/10.1029/2012WR011965

A new model for the spectral induced polarization signature of bacterial growth in porous media

A. Revil,[1,2] E. Atekwana,[3] C. Zhang,[4] A. Jardani,[5] and S. Smith[6]

Received 6 February 2012; revised 2 August 2012; accepted 2 August 2012; published 27 September 2012.

[1] The complex conductivity of porous materials and colloidal suspensions comprises two components: an in-phase conductivity associated with electromigration of the charge carriers and a quadrature conductivity associated with the reversible storage of the charges at some polarization length scales. We developed a quantitative model to investigate the frequency domain induced polarization response of suspensions of bacteria and bacteria growth in porous media. Induced polarization of bacteria (α polarization) is related to the properties of the electrical double layer of the bacteria. Surface conductivity and α polarization are due to the Stern layer of counterions occurring in a brush of polymers coating the surface of the bacteria. These phenomena can be related to their cation exchange capacity. The mobility of the counterions in this Stern layer is found to be very small (4.7×10^{-10} m^2 s^{-1} V^{-1} at 25°C). This implies a very low relaxation frequency for the α polarization of the bacteria cells (typically around 0.1–5 Hz), in agreement with experimental observations. This new model can be coupled to reactive transport modeling codes in which the evolution of bacterial populations are usually described by Monod kinetics. We show that the growth rate and endogenous decay coefficients of bacteria in a porous sand can be inferred nonintrusively from time-lapse frequency domain induced polarization data.

Citation: Revil, A., E. Atekwana, C. Zhang, A. Jardani, and S. Smith (2012), A new model for the spectral induced polarization signature of bacterial growth in porous media, *Water Resour. Res.*, *48*, W09545, doi:10.1029/2012WR011965.

1. Introduction

[2] In situ bioremediation experiments have recently been successfully monitored through time-lapse geophysical methods [*Williams et al.*, 2005, 2009]. Two methods have been shown to be sensitive to the growth of bacterial: the self-potential method [*Revil et al.*, 2010] and the induced polarization method [*Atekwana and Slater*, 2009]. In the present work, we are concerned with this second approach. At high frequencies (>100 kHz), polarization is dielectric in nature. However, at low frequencies, polarization is due to the reversible storage of electrical charges moving under the influence of the external electrical field and being stored at some polarization length scales. In the present paper, we are especially interested in understanding quantitatively the relationship between frequency domain induced polarization and bacterial growth and decay in porous media with the possible end goal to use recently developed time-lapse frequency domain or time domain induced polarization tomography [*Karaoulis et al.*, 2011] to monitor this process in laboratory and field conditions.

[3] The measurement principle of frequency domain induced polarization is based on the injection/retrieval of a harmonic current using two electrodes and the measurement of the resulting electrical field with two other electrodes. Ohm's law can be used to determine the magnitude of the electrical conductivity at a given frequency of the external electrical field or applied current. A phase lag can also be measured between the electrical field and the applied current. The magnitude of the electrical conductivity and the phase lag can be written as a complex conductivity with an in-phase (real) component and a quadrature (imaginary) component. For abiotic porous media, low-frequency polarization mechanisms are generally associated with the existence of the electrical double layer coating the surface of the minerals [*Vaudelet et al.*, 2011a, 2011b].

[4] Bacteria, like minerals in contact with water, are coated with electrical double layer. At near-neutral pH values, both gram-positive and gram-negative bacteria have a net negative charge on the surface of their membrane [e.g., *van der Wal et al.*, 1997a, 1997b; *Grosse*, 2002; *Dittrich and Sibler*, 2005], which attracts cations and repels anions. In addition, their activity can alter local redox conditions [e.g., *Personna et al.*, 2008]. Therefore it is not surprising that induced polarization could be an effective tool to nonintrusively monitor bacterial growth in porous media. *Davis et al.* [2006] showed that the formation of biofilms in a porous sand changes its

[1]Department of Geophysics, Colorado School of Mines, Golden, Colorado, USA.
[2]ISTerre, CNRS UMR 5275, Université de Savoie, Le Bourget du Lac, France.
[3]Boone Pickens School of Geology, Oklahoma State University, Stillwater, Oklahoma, USA.
[4]Idaho National Laboratory, Idaho Falls, Idaho, USA.
[5]Morphodynamique Continentale et Côtière, CNRS UMR 6143 M2C, Université de Rouen, Mont-Saint-Aignan, France.
[6]Chevron Energy Technology Company, Houston, Texas, USA.

Corresponding author: A. Revil, Department of Geophysics, Colorado School of Mines, Green Center, 1500 Illinois St., Golden, CO 80401, USA. (arevil@mines.edu)

0043-1397/12/2012WR011965

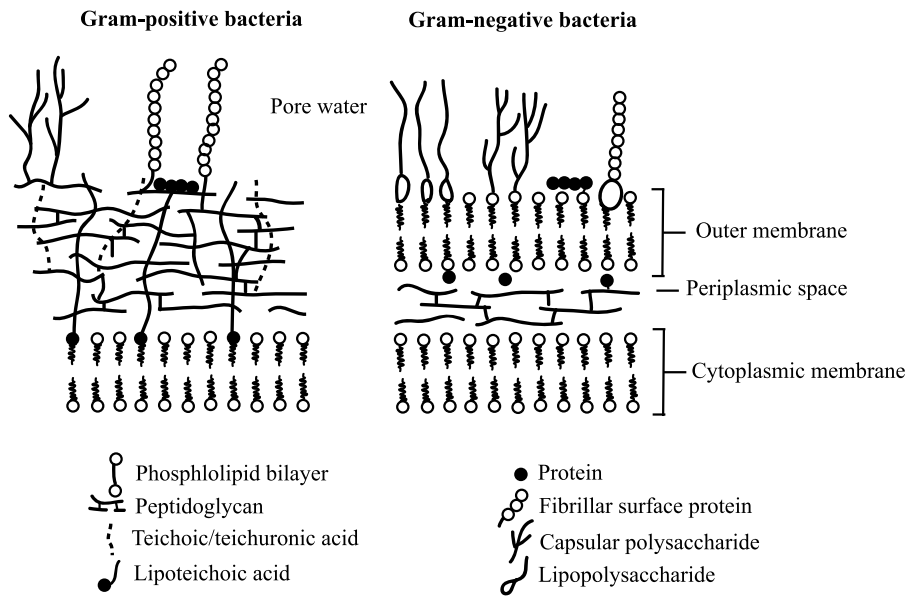

Figure 1. Sketch of the surface of gram-positive and gram-negative bacteria (not to scale). From this sketch, it follows that the surface charge of the bacteria is located in a three-dimensional network of polymers extending outward from the surface of the insulating membrane of the bacteria. The conductivity of the cytoplasmic membrane is smaller than 10^{-6} S m^{-1}, and its thickness very small (<10 nm).

quadrature conductivity [*Abdel Aal et al.*, 2010; *Ntarlagiannis et al.*, 2005a]. *Albrecht et al.* [2011] showed a strong phase shift change (~50 mrad) associated with the formation of a biofilm of *Burkholderia* sp. in a phenanthrene-contaminated sand. The presence of bacteria can also be detected indirectly through the induced polarization responses associated with byproducts of the microbial activities such as precipitation of sulfides [*Ntarlagiannis et al.*, 2005b; *Slater et al.*, 2007; *Personna et al.*, 2008]. In the present paper, we do not examine the induced polarization signature associated with the precipitation of sulfide or magnetite. We focus instead on the role of the bacteria themselves upon induced polarization in the absence of biomineralization.

[5] So far, only observations have been reported in biogeophysics regarding the signature of bacteria in porous media upon induced polarization. In contrast, in colloidal chemistry, the electrical properties of suspensions of bacteria have been measured and modeled for a long time and both at high frequencies (>0.1 MHz), using dielectric spectroscopy, and at low frequencies (<0.1 MHz) using AC impedance spectroscopy. Several mechanisms of polarization have been observed.

[6] 1. In the gigahertz to terahertz range, three γ polarization mechanisms dominate. One is due to the relaxation of the bulk pore water, the second is due to the relaxation of the bound water coating the surface of the bacteria, and the third is due to the difference of permittivity between the bacterial cells and the electrolyte [*Grosse*, 2002].

[7] 2. In the megahertz range, the β polarization represents the major contribution to polarization. It corresponds to the Maxwell-Wagner (interfacial polarization) of the membrane of the bacteria [*Irimajiri et al.*, 1987; *Ferris et al.*, 1990].

[8] 3. At low frequencies (<100 kHz), the so-called α polarization prevails [*Grosse*, 2002]. This polarization mechanism is associated with the polarization of the electrical double layer coating the surface of the bacteria [*Grosse*, 2002].

[9] We will not model the high-frequency β and γ polarization mechanisms in this paper. Indeed, we are mostly interested in describing the low-frequency α polarization (<0.1 MHz) because of its application to induced polarization geophysics. Also the β polarization is not always visible in the polarization of suspensions of bacteria because of the small size of these cells [*Irimajiri et al.*, 1987; *Ferris et al.*, 1990]. In the present paper, we provide therefore a model for the α polarization of suspensions of bacteria to evaluate quantitatively changes in the complex conductivity of porous media during bacterial growth over time.

2. Polarization of Bacteria

[10] In this section, we describe the surface electrochemical properties of the bacteria in contact with water. We describe in section 2.1. the bacterial cation exchange capacity and in section 2.2. the surface charging mechanisms of the carboxyl, phosphate, and amino surface groups in the polymeric brush made of fibrillar surface protein, capsular polysaccharide, and lipopolysaccharide molecules coating the surface of bacteria. Like for clays, most of the counterions are contained in the Stern layer. In section 2.3., we describe a new polarization model for a suspension of bacteria.

2.1. Cation Exchange Capacity

[11] The low-frequency induced polarization of clays seems to be due to the Stern layer coating the surface of the clay particles. We argue that bacteria have a similar charging mechanism (amphoteric surface reactions and weak sorptions of counterions associated with the carboxyl, phosphate, and amino surface groups). The main property of this double layer (Stern plus diffuse layers) is the cation exchange

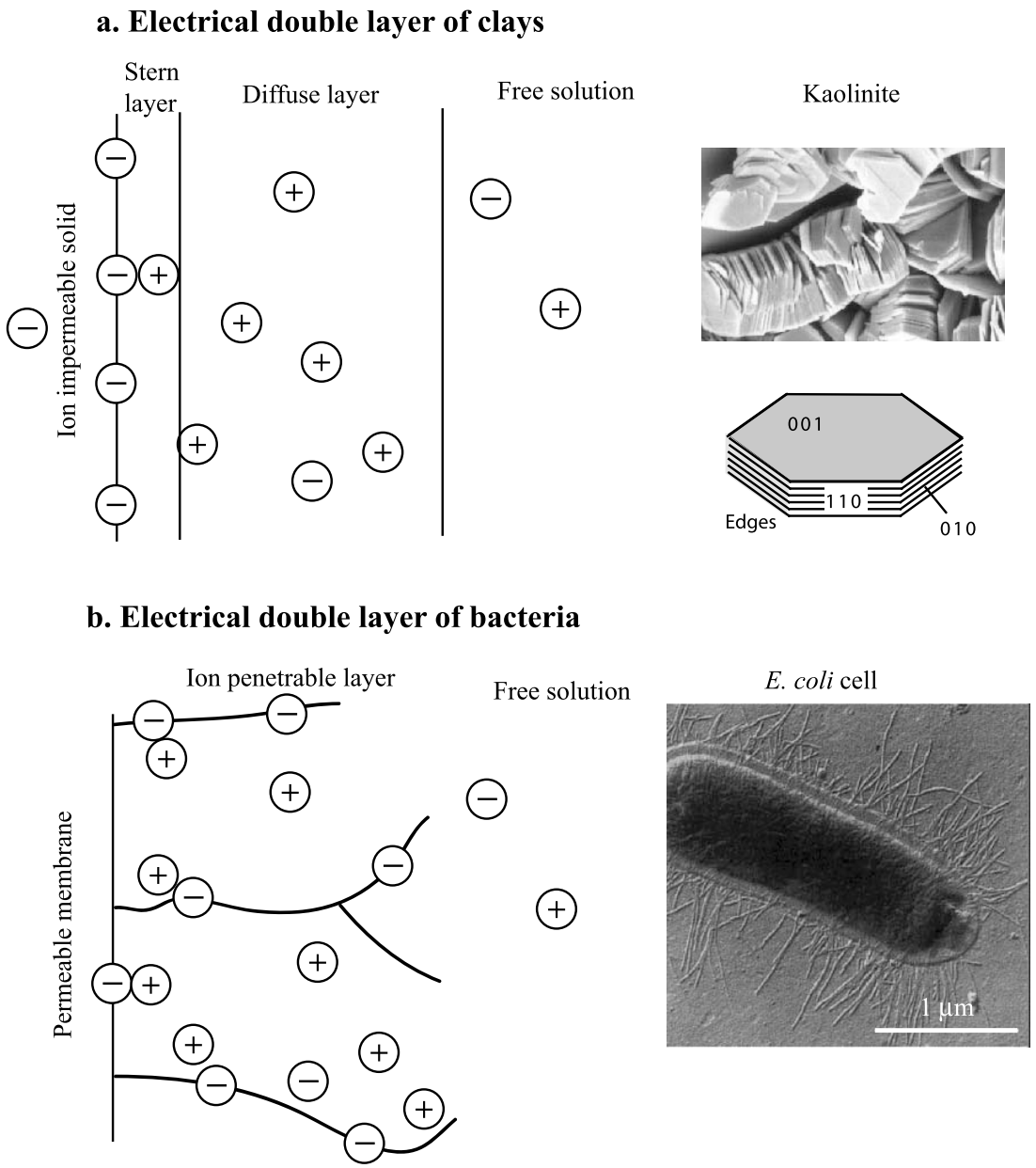

Figure 2. Difference between the electrical double layer (EDL) of clays or silica and the electrical double layer of bacteria cell. (a) The EDL of clays occurs on a relatively flat surface with both a Stern layer and a diffuse layer. (b) The EDL of bacteria occurs inside a polyelectrolyte coating the membrane surface, and the counterions are located in a diffuse layer (picture *E. coli*).

capacity (CEC). We first focus our analysis on the excess charge per unit pore volume associated with the presence of bacteria. The charge per unit pore volume of a colloidal suspension of bacteria is (in C m^{-3}):

$$Q_V^B \equiv \sum_{i=1}^{M} C_i^B \mathrm{CEC}_i^B. \quad (1)$$

where CEC_i^B denotes the cation exchange capacity of bacteria type i (in C kg^{-1}), M denotes the number of different types of bacteria, and C_i^B denotes the concentration of bacteria (in kg per m^{-3} of pore water solution). The CEC of the thermophilic bacterium *Anoxybacillus flavithermus* is for instance 0.3 mmol (or meq) $g^{-1} = 29 \times 10^3$ C kg^{-1} where C stands for Coulomb [*Heinrich et al.*, 2007]. This value is comparable to the value of illite (0.2 ± 0.1 mmol/g [e.g., *Leroy and Revil*, 2009]). The high charge density of bacteria is usually associated with the 3D organization of these charges on their membrane (Figure 1) [see *Poortinga et al.*, 2002]. The surface of bacteria is similar to that of a polyelectrolyte [*Ohshima*, 2002] implying a high surface charge density on their surface (Figures 1 and 2). From a modeling point of view, Figure 1 implies clearly that the surface of the bacteria cannot be modeled as a smooth surface.

[12] Another way to compare the charge density of bacteria and clays is to look at their effective surface charge

Table 1. Specific Surface Area and Cation Exchange Capacity of Some Gram-Positive and Gram-Negative Bacteria[a]

Bacterium Type	Bacterium	Surface Area[b] (m^2/g)	CEC[b] (mmol/g live cells)
Gram-positive	*Bacillus subtilis*	140 (1)	4.52 (3)
Gram-positive	*Corynebacterium* DSM44016	62 (2)	2.00 (2)
Gram-positive	*Corynebacterium* DSM6688	103 (2)	3.22 (2)
Gram-positive	*Rhodococcus erythropolis*	90 (2)	1.94 (2)
Gram-positive	*R. opacus*	100 (2)	1.56 (2)
Gram-positive	*Bacillus brevis*	28 (2)	3.48 (2)
Gram-positive	*B. licheniformis*		6.00 (3)
Gram-negative	Syn. green		1.38 (3)
Gram-negative	Syn. red		3.32 (3)
Gram-negative	*Enterobacteriaceae*		2.64 (3)
Gram-negative	*Shewanella putrefaciens*		0.16 (3)
Gram-negative	*Calothrix* cell		2.92 (3)
Gram-negative	*Calothrix* sheath		0.36 (3)
Gram-negative	*Escherichia coli* D21g		0.25 (4)
Cyanobacteria	*Microcystis aeruginosa*[c]		1.60 (5)
Algae	*C. vulgaris aeruginosa*[d]		0.22 (5)

[a]The CEC is reported per mass of living bacteria around neutral pH values (we have converted the CEC per gram of dry bacteria to per gram of hydrated bacteria by using a dry weight to wet weight ratio W of 0.5). Note that, in general, the CEC of gram-positive bacteria is higher than the CEC of gram-negative bacteria (3.08 mmol/g versus 1.80 mmol/g).

[b]Numbers in parentheses indicate the following sources: 1, *Leone et al.* [2007]; 2, *van der Wal et al.* [1997a]; 3, *Dittrich and Sibler* [2005, Table 3]; 4, *Walker et al.* [2005], growth phase; 5, *Hadjoudja et al.* [2010], growth phase.

[c]*Microcystis aeruginosa* is a cyanobacteria. Its walls are stained gram-positive, but the cell appears gram negative.

[d]*Chlorella vulgaris* is a species of single-celled green algae.

densities. According to *van der Wal et al.* [1997a], the surface charge density of gram-positive bacteria is in the range 0.5–1.0 C m^{-2} corresponding to 3 to 6 elementary charges per nm^2. This range of values is higher than for clays (usually 1 to 3 elementary charges per nm^2 [see *Leroy and Revil*, 2009]. The specific surface area and CEC of some gram-positive and gram-negative bacteria are reported in Table 1. As a side note, the CEC is usually given in moles or charge (in C) per unit dry mass. The dry weight to wet weight ratio W for a broad number of bacteria is usually 0.31 to 0.57 according to *Bratbak and Dundas* [1984]. An average value of 0.50 can be used to convert the values provided per unit dry mass into charge per unit mass of living bacteria (by dividing the values of the CEC per unit dry mass by the factor W).

2.2. The Electrical Double Layer of Bacteria

[13] Like for clays, one can write a speciation model for the surface sites responsible for an electrical double layer at the surface of bacteria. For example, the surfaces of gram-positive bacteria contain peptidoglycan, whose molecule is rich in three types of reactive charged surface groups: carboxylic acid (>COOH), amine (>NH^+), and phosphate (>PO^-) (> means that the functional group is attached to the cell wall structure of the bacterium [*Leone et al.*, 2007]). For the gram-positive bacterium investigated by *Leone et al.* [2007], the relative proportion of these sites is 1.2:1:0.9. The protonation-deprotonation of these groups can be written as

$$> \mathrm{COOH}^0 \Leftrightarrow > \mathrm{COO}^- + \mathrm{H}^+, K_1 = 10^{-3.8}, \quad (2)$$

$$> \mathrm{NH}_3^+ \Leftrightarrow > \mathrm{NH}_2^0 + \mathrm{H}^+, K_2 = 10^{-6.1}, \quad (3)$$

$$> \mathrm{PO}_4^- + \mathrm{H}^+ \Leftrightarrow > \mathrm{PO_4H}^0, K_3 = 10^{2.2}. \quad (4)$$

[14] Some of the carboxylic acid, amine, and phosphate groups can have different dissociation constants than above, in equations (2) to (4), depending on the molecules they are attached to. Gram-negative cells, on the other hand, contain lipopolysaccharides instead of peptidoglycan. Lipopolysaccharides also contain charged phosphate and carboxyl groups. Table 2 lists the common charged surface compounds found in both gram-positive and gram-negative bacteria.

[15] We take the analogy between clays and bacteria one step further. The electrical double layer of clays is formed by a Stern layer including weakly sorbed counterions (forming outer-sphere complexes) and a diffuse layer in which the cations and anions are only related to the charge of the mineral surface through Coulombic interactions. *Revil* [2012] showed that most of the countercharge of clays is located in the Stern layer (>85%), and that the Stern layer plays a major role in the induced polarization of clay-rich materials.

[16] The description of the Stern layer of bacteria requires a more sophisticated set of complexation reactions than the amphoteric reactions corresponding to equations (2) to (4). In addition to the protonation reactions listed, the sorption of metallic cations, e.g., M^+ (Na^+ or K^+ for instance) can be modeled by the following reactions involving sorption of the

Table 2. Speciation at the Surface of Bacteria

Reaction	Molecule	Site Type	pKa[a] (25°C)
$> \mathrm{COOH}^0 \Leftrightarrow > \mathrm{COO}^- + \mathrm{H}^+$	Polysaccharide	1	2.8
$> \mathrm{COOH}^0 \Leftrightarrow > \mathrm{COO}^- + \mathrm{H}^+$	Protein, peptidoglycan	2	4.0–5.0
$> \mathrm{NH}_3^+ \Leftrightarrow > \mathrm{NH}_2^0 + \mathrm{H}^+$	Protein, peptidoglycan	3	9.0–9.8
$> \mathrm{HPO}_4^0 \Leftrightarrow > \mathrm{PO}_4^- + \mathrm{H}^+$	Teichoic acids	4	2.1
$> \mathrm{H_2PO}_4^0 \Leftrightarrow > \mathrm{HPO}_4^- + \mathrm{H}^+$	Phospholipids	5	2.1
$> \mathrm{HPO}_4^{-1} \Leftrightarrow > \mathrm{PO}_4^{2-} + \mathrm{H}^+$	Phospholipids	6	7.2

[a]Here pKa represents the -log10 value of the dissociation constants [from *Poortinga et al.*, 2002].

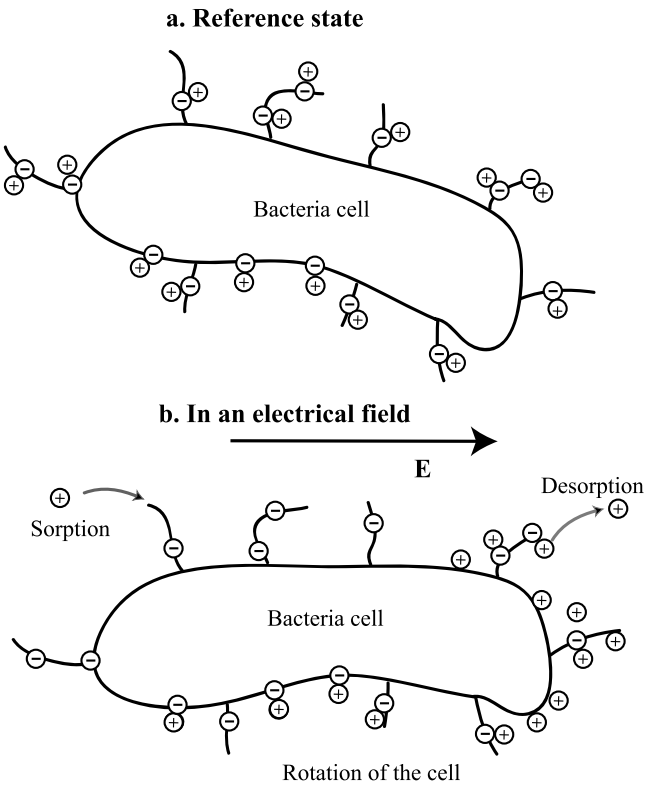

Figure 3. Sketch of the α-type polarization of the bacteria cell. The migration of the counterions in the direction of the electrical field is responsible for a dipole moment associated with the cell. Note that the cells themselves try to align with the electrical field, and therefore, there is an electrorotation of the cells in the field. Finally, during the polarization of the cell, cations get sorbed and desorbed, which corresponds to a leaking capacitance, justifying the use of the Warburg impedance model to describe the polarization of the cell.

counterions in the Stern layer of the surface of the bacteria [e.g., *Daughney and Fein*, 1998],

$$> COO^-M^+ \Leftrightarrow > COO^- + M^+, \tag{5}$$

$$> NH_2M^+ \Leftrightarrow > NH_2^0 + M^+, \tag{6}$$

$$> PO_4^-M^+ \Leftrightarrow > PO_4^- + M^+. \tag{7}$$

[17] This sorption is weak and does not involve covalent bounds. The implication of these equations is of paramount importance to our model for three reasons.

[18] 1. Sorption of some metal ions (e.g., Na^+ or K^+) on the surface of bacteria occurs mostly as outer-sphere complexes which means that these counterions in the Stern layer are mobile in an electrical field. Then at some point, we will need to determine their mobility later on.

[19] 2. The sorption and desorption of these counterions during the polarization of the cells is possible like for clays. In the case, there is no sorption/desorption during the polarization of the cells, the complex conductivity can be described by a Debye model [*Schwarz*, 1962; *Leroy et al.*, 2008] and the role of the double layer corresponds to a perfect capacitance. Sorption/desorption implies that the electrical double layer behaves as a "leaking" capacitance. Such leaking capacitance behavior has been described in the literature [*Wong*, 1979] and can be described by a Warburg impedance model [*Warburg*, 1899].

[20] 3. *van Der Wal et al.* [1997b] have inferred that most of the counterions surrounding bacteria are located in the Stern layer and not in the diffuse layer. This means that the classical mathematical treatment of the α polarization of such cells may be inadequate because based on a diffuse layer model. We provide below a simple model based on the Stern layer model (Figure 3).

2.3. General Model

[21] We are looking first for some expressions for the effective conductivity and permittivity of a suspension of bacteria (Figure 4). Ampère law is given by

$$\nabla \times \mathbf{H} = \mathbf{J} + \frac{\partial \mathbf{D}}{\partial t}, \tag{8}$$

where t is time (in s), $\mathbf{J}$ is the conduction (electromigration) current density, $\mathbf{J}_d = \partial \mathbf{D}/\partial t$ denotes the displacement current density (both in A m^{-2}), $\mathbf{H}$ is the magnetic field (expressed in A m^{-1}), $\mathbf{D} = \varepsilon \mathbf{E}$ is the dielectric displacement (in C m^{-2}), and ε is the permittivity (in F m^{-1}) of the material. In linear models, the current density is given by a linear Ohm's law, $\mathbf{J} = \sigma^* \mathbf{E}$ with the harmonic electrical field $\mathbf{E} = \mathbf{E}_0 \exp(-i\omega t)$ ($i = \sqrt{-1}$ the pure imaginary number, $\omega = 2\pi f$ the angular frequency (in rad s^{-1}) of the external electric field, f is the frequency in Hz, and $\mathbf{E}_0$ is a constant electrical field magnitude and direction). The total (subscript t) current density is the sum of the conduction current and displacement current densities. This yields $\mathbf{J}_t = (\sigma^* - i\omega\varepsilon)E$ [*Vinegar and Waxman*, 1984], where σ^* denotes the complex conductivity, $\sigma^* = \sigma' + i\sigma''$. The total current density can be written as

$$\mathbf{J}_t = \sigma_{eff}^* \mathbf{E}, \tag{9}$$

where $\sigma_{eff}^* = \sigma_{eff} - i\omega\varepsilon_{eff}$ is the effective complex conductivity and σ_{eff} and ε_{eff} are real scalars dependent upon frequency. These effective parameters are the parameters that are measured during an experiment in the laboratory. They contain both electromigration and true dielectric polarization effects,

$$\sigma_{eff} = \sigma', \tag{10}$$

$$\varepsilon_{eff} = \varepsilon' - \sigma''/\omega. \tag{11}$$

[22] We describe now a specific model of polarization for the effective conductivity and permittivity of the material. This model is shown in Figure 4 and developed further in Appendix A. We assume that (1) the dielectric constant of the polymeric brush is close to the dielectric constant of the electrolyte and (2) that the conductivity of the membrane of the cell is zero (see discussion in Appendix A). The conductivity of a suspension of cells is therefore controlled by the amount of bacteria and the surface conductivity of the brush of polymers coating their surface.

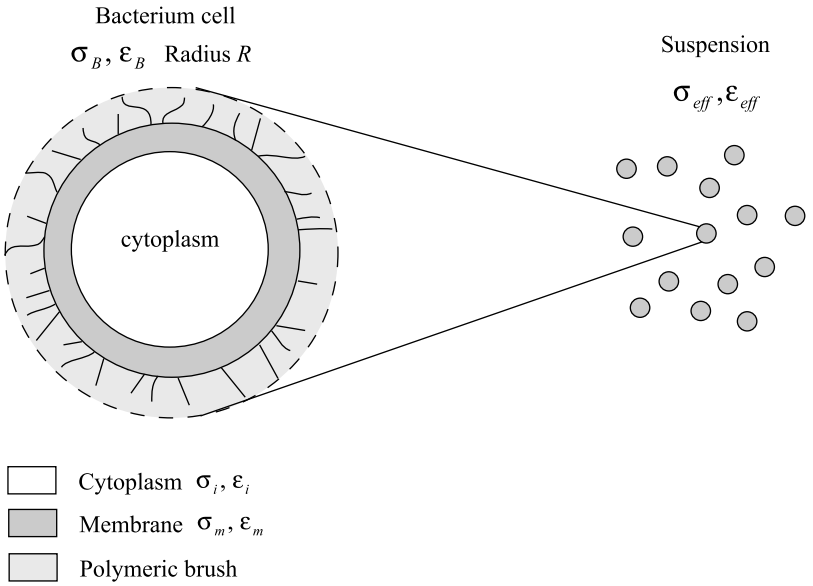

Figure 4. Sketch of the geometry of the bacteria used to build the polarization model. The cell is formed by a cytoplasm surrounded by two thin shells: the membrane and an outer shell formed by the three-dimensional network of polymers extending outward from the surface of the membrane of the bacteria.

[23] *Wong* [1979] provided a model describing the polarization of conductive (sulfide) particles exchanging charge carriers with the surrounding pore water. In this case, the frequency-dependent complex conductivity can be described by a Warburg impedance model (the Warburg component describes the leaking capacitance associated with the polarization of the electrical double layer). We follow this idea and use a Cole-Cole model to describe the α polarization of a suspension of bacteria:

$$\sigma^*(\omega) = \sigma_\infty \left[1 - \frac{M}{1 + (i\omega\tau)^c}\right], \tag{12}$$

where $\tau = 1/(2\pi f_c)$ denotes the main relaxation time (in s) (also called time constant by some geophysicists), f_c denotes the associated critical frequency, and c denotes the Cole-Cole exponent. The Warburg model corresponds to the special case $c = 0.5$. In equation (12), the chargeability M is computed from the ratio of the high- and low-frequency conductivity of the suspension of bacteria (σ_∞ and σ_0)

$$M = 1 - \frac{\sigma_0}{\sigma_\infty}. \tag{13}$$

The real and imaginary parts of the complex conductivity of the Cole-Cole model are given by

$$\sigma' = \sigma_\infty + \frac{1}{2}(\sigma_0 - \sigma_\infty)\left\{1 - \frac{\sinh[c\ln(\omega\tau)]}{\cosh[c\ln(\omega\tau)] + \cos\left[\frac{\pi}{2}(1-c)\right]}\right\}, \tag{14}$$

$$\sigma'' = \frac{1}{2}\left\{\frac{(\sigma_0 - \sigma_\infty)\cos\left[\frac{\pi}{2}(1-c)\right]}{\cosh[c\ln(\omega\tau)] + \sin\left[\frac{\pi}{2}(1-c)\right]}\right\}. \tag{15}$$

From equations (10) to (15), the effective conductivity and dielectric constant are expressed as

$$\sigma_{eff} = \sigma_\infty + \frac{1}{2}(\sigma_0 - \sigma_\infty)\left\{1 - \frac{\sinh[c\ln(\omega\tau)]}{\cosh[c\ln(\omega\tau)] + \cos\left[\frac{\pi}{2}(1-c)\right]}\right\}, \tag{16}$$

$$\varepsilon_{eff} = \varepsilon' - \frac{1}{2\omega}\left\{\frac{(\sigma_0 - \sigma_\infty)\cos\left[\frac{\pi}{2}(1-c)\right]}{\cosh[c\ln(\omega\tau)] + \sin\left[\frac{\pi}{2}(1-c)\right]}\right\}, \tag{17}$$

respectively. The effective relative permittivity is given by dividing equation (17) by the dielectric constant of vacuum $\varepsilon_0 = 8.85 \times 10^{-12}$ F m^{-1} and $K = \varepsilon'/\varepsilon_0$ denotes the permittivity of the suspension and $K_{eff} = \varepsilon_{eff}/\varepsilon_0$ denotes its effective permittivity.

[24] We need now to find some expressions for ε', σ_∞, and σ_0. Regarding the surface conductivity, we need to assess what fraction f of the counterions is located in the Stern layer and what fraction $(1 - f)$ of the counterions is located in the diffuse layer. In agreement with *van der Wal et al.* [1997b], we assume that nearly all the counterions are located in the Stern layer (therefore, $f \approx 1$). For a suspension of bacteria, we assume that surface conductivity is zero at very low frequency ($\sigma_S^0 = 0$ for $\omega \ll 1/\tau$) and all the Stern layer participates to surface conduction at very high frequencies (the high frequency $\omega \gg 1/\tau$, is denoted as σ_S^∞). The membrane of the cell is insulating (see Appendix A) and therefore the electrical conductivity of the bacteria is only due to conduction in the brush of polymers coating their surface. With these assumptions, we obtain (see Appendix A),

$$\sigma_\infty = \frac{1}{F_B}\left(\sigma_w + m_B\beta_{(+)}Q_V^B\right), \tag{18}$$

$$\sigma_0 = \frac{1}{F_B}\sigma_w, \tag{19}$$

$$\varepsilon' = \frac{1}{F_B}[\varepsilon_w + (F_B - 1)\varepsilon_B], \tag{20}$$

where σ_w and ε_w denote the conductivity and dielectric constant of the pore water, respectively, F_B denotes the formation factor associated with the presence of the bacteria, m_B denotes the cementation exponent, and $\beta_{(+)}$ denotes the mobility of the counterions in the Stern layer. The dielectric constant of the cell is typically given by $\varepsilon_B \approx 6\varepsilon$ [*Grosse*, 2002]. Because $(F_B - 1)\varepsilon_B = \bar{V}_B\bar{C}_B\varepsilon_B$ in the dilute approximation, the dielectric constant is proportional to the density of cells, which is in agreement with the observations of *Siano* [1997].

[25] The crucial parameter describing polarization is the normalized chargeability defined by

$$M_n = M\sigma_\infty = \sigma_\infty - \sigma_0. \tag{21}$$

[26] Equations (18), (19), and (21) yield the following simple expression for the normalized chargeability:

$$M_n = \frac{1}{F_B} m_B \beta_{(+)} Q_V^B. \tag{22}$$

[27] The term $(\sigma_0 - \sigma_\infty)$ in equations (16) and (17) can be replaced by $(-M_n)$ making clear that the frequency-dependent terms in the effective quadrature conductivity ($\sigma''_{eff} = \omega\sigma_{eff}$) and the effective conductivity and dielectric constant are controlled by the normalized chargeability.

[28] We can now express the excess charge density in terms of the cation exchange capacity of the bacteria using equations (1) and (22) and using only a single bacteria species. This yields

$$M_n = \frac{1}{F_B} m_B \beta_{(+)} C_B \mathrm{CEC}_B. \tag{23}$$

[29] Usually, the concentration of bacteria is not reported in kg per m^{-3} of pore water solution but in cell density. The relationship between these two concentrations is given by

$$C_B = \bar{C}_B \bar{V}_B \rho_B, \tag{24}$$

where ρ_B represents the mass density of active bacteria ($\sim$1010 to 1020 kg m^{-3} [*Bratbak and Dundas*, 1984]), $\bar{V}_B$ denotes the volume of a single bacterium (the cell volume $\bar{V}_B$ is typically in the range 0.5 to 1.0 μm^3), and $\bar{C}_B$ denotes the number of bacteria per unit pore volume (in m^{-3}) defined by

$$\bar{C}_B = N_B/V, \tag{25}$$

where N_B is the number of bacteria and V the volume of the colloidal suspension. Combining equations (23) and (24), we obtain the following equation for the normalized chargeability for bacteria:

$$M_n = \frac{m_B}{F_B}\left(\beta_{(+)} \bar{V}_B \rho_B \mathrm{CEC}_B\right)\bar{C}_B. \tag{26}$$

[30] The evolution of the normalized chargeability is thus a direct measurement of the bacteria density.

[31] Three points are important to consider in order to test our model.

[32] 1. In dilute solutions (F_B = 1), the quadrature conductivity and the normalized chargeability are proportional to the cation exchange capacity of the bacteria and the mobility of the counterions in the electrical double layer coating the bacteria.

[33] 2. Because of equations (15) and (26), the quadrature conductivity response is expected to depend linearly on the bacteria cell density. Therefore, a relative change of quadrature conductivity should be equal to a relative change in bacterial density (deviation from linearity may be expected for high concentrations of bacteria because of its effect on the formation factor, F_B). This is consistent with the observations reported by *Abdel Aal et al.* [2004] and *Albrecht et al.* [2011]. *Albrecht et al.* [2011] showed the existence of a linear relationship between the volume of biofilm (which may be proportional to first approximation to the bacteria density) and the phase lag for *Burkholderia* sp. (strain NAH1, a rod-shaped gram-negative bacteria).

[34] 3. The final expressions for the effective conductivity and permittivity are given by,

$$\sigma_{eff} = \sigma_\infty - \frac{1}{2}M_n\left\{1 - \frac{\sinh[c\ln(\omega\tau)]}{\cosh[c\ln(\omega\tau)] + \cos\left[\frac{\pi}{2}(1-c)\right]}\right\}, \tag{27}$$

$$K_{eff} = K' + \left(\frac{M_n}{2\omega\varepsilon_0}\right)\frac{\cos\left[\frac{\pi}{2}(1-c)\right]}{\cosh[c\ln(\omega\tau)] + \sin\left[\frac{\pi}{2}(1-c)\right]}. \tag{28}$$

[35] In addition, we can also plot the apparent imaginary (quadrature) conductivity given by

$$\sigma''_{eff} \equiv \omega\varepsilon_0 K_{eff} = \sigma'' + \omega\varepsilon'. \tag{29}$$

[36] In equations (27) and (28), ε' and σ_∞ are given by,

$$\varepsilon' = \frac{1}{F_B}(\varepsilon_w + m_B\bar{C}_B\bar{V}_B\varepsilon_B), \tag{30}$$

$$\sigma_\infty = \frac{1}{F_B}\left[\sigma_w + \left(m_B\beta_{(+)}\bar{V}_B\rho_B\mathrm{CEC}_B\right)\bar{C}_B\right], \tag{31}$$

and the normalized chargeability by equation (26). The relaxation time is given from the model of relaxation of the electrical double layer where d_B denotes the mean diameter of the bacteria (diameter of an equivalent volume with the same volume than the bacteria). This yields [*Wong*, 1979],

$$\tau = \frac{{d_B}^2}{8D_{(+)}} = \frac{{d_B}^2 e}{8k_b T\beta_{(+)}}, \tag{32}$$

where τ is a relaxation time (in s) d_B is the mean size of the bacteria cell (diameter of a sphere of same volume of the bacteria, typically 1 to 3 μm), $D_{(+)}$ is the diffusion coefficient of the counterions in the Stern layer. This diffusion coefficient is related to the mobility of the counterions in the Stern layer, $\beta_{(+)}$, by the Nernst-Einstein relationship $D_{(+)} = k_b T\beta_{(+)}/|q_{(+)}|$ (k_b is the Boltzmann constant (1.3807×10^{-23} J K^{-1}), T is the absolute temperature, and $|q_{(+)}|$ is the absolute value of the charge of the counterions). For a typical bacterial cell, using the value of $\beta_{(+)}$ given below in section 3 at 25°C (4.7×10^{-10} m^2 s^{-1} V^{-1}), and using d_B = 3 μm yields τ = 0.1 s (1.6 Hz). If we use d_B = 1 μm instead, we obtain τ = 0.01 s (16 Hz). We obtain high relaxation times and therefore low relaxation frequencies. The high- and low-frequency

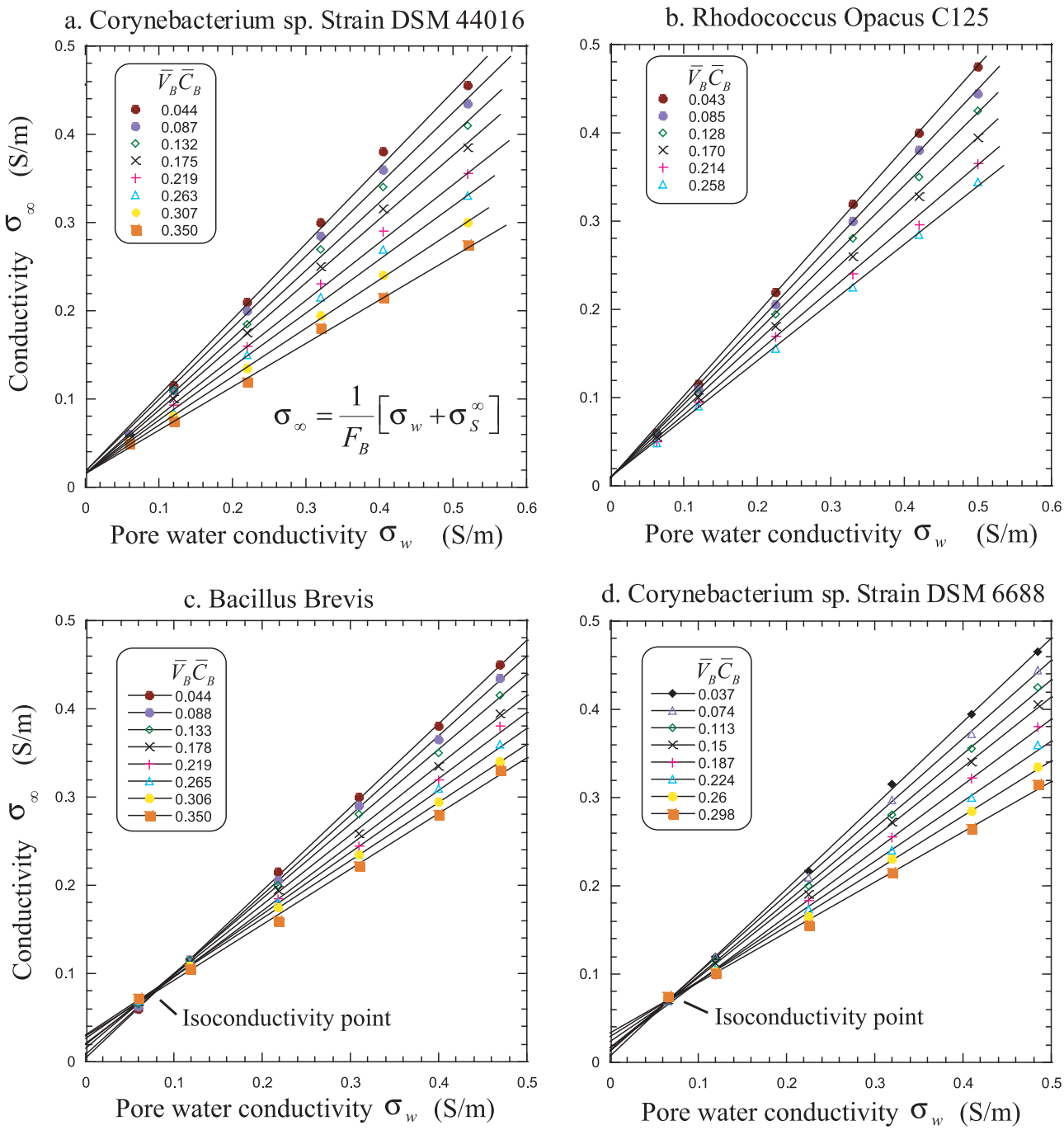

Figure 5. Analysis of the conductivity of suspensions of bacteria. The plots correspond to the conductivity of the suspension versus the conductivity of the pore water for different bacteria and different values of the volumetric fraction of bacteria. For each volume fraction of bacteria, we fit the data to obtain the formation factor and the surface conductivity. Data are from *van der Wal et al.* [1997b], and pH = 6.5–7.0.

regimes for the electrical conductivity will be defined with respect to this relaxation frequency.

3. Polarization of a Colloidal Suspension of Bacteria

3.1. Electrical Conductivity

[37] We first test the expression of the electrical conductivity using the data set of *van der Wal et al.* [1997b] for various gram-positive bacteria including *Corynebacterium sp.* strain DSM 44016 (spherical, length 1.1 μm, width, 0.8 μm), *Corynebacterium* sp. strain DSM 6688 (rod shaped, length 2.0 μm, width, 0.6 μm), *Rhodococcus opacus* C125 (rod shaped, length 3.2 μm, width 1.2 μm), *Bacillus brevis* (rod shaped, length 6.0 μm, width 1.0 μm), and *Rhodococcus erythropolis* A177 (rod shaped, length 2.9 μm, width 1.9 μm). The CEC of these bacteria are reported in Table 1. Their electrical conductivity data are shown in Figure 5. They were measured at 25°C, KNO_3 solutions with molarity of 0.05, 0.04. 0.03, 0.02, 0.01 and 0.005 M, pH 6.5–7.0, and at 3.7 kHz

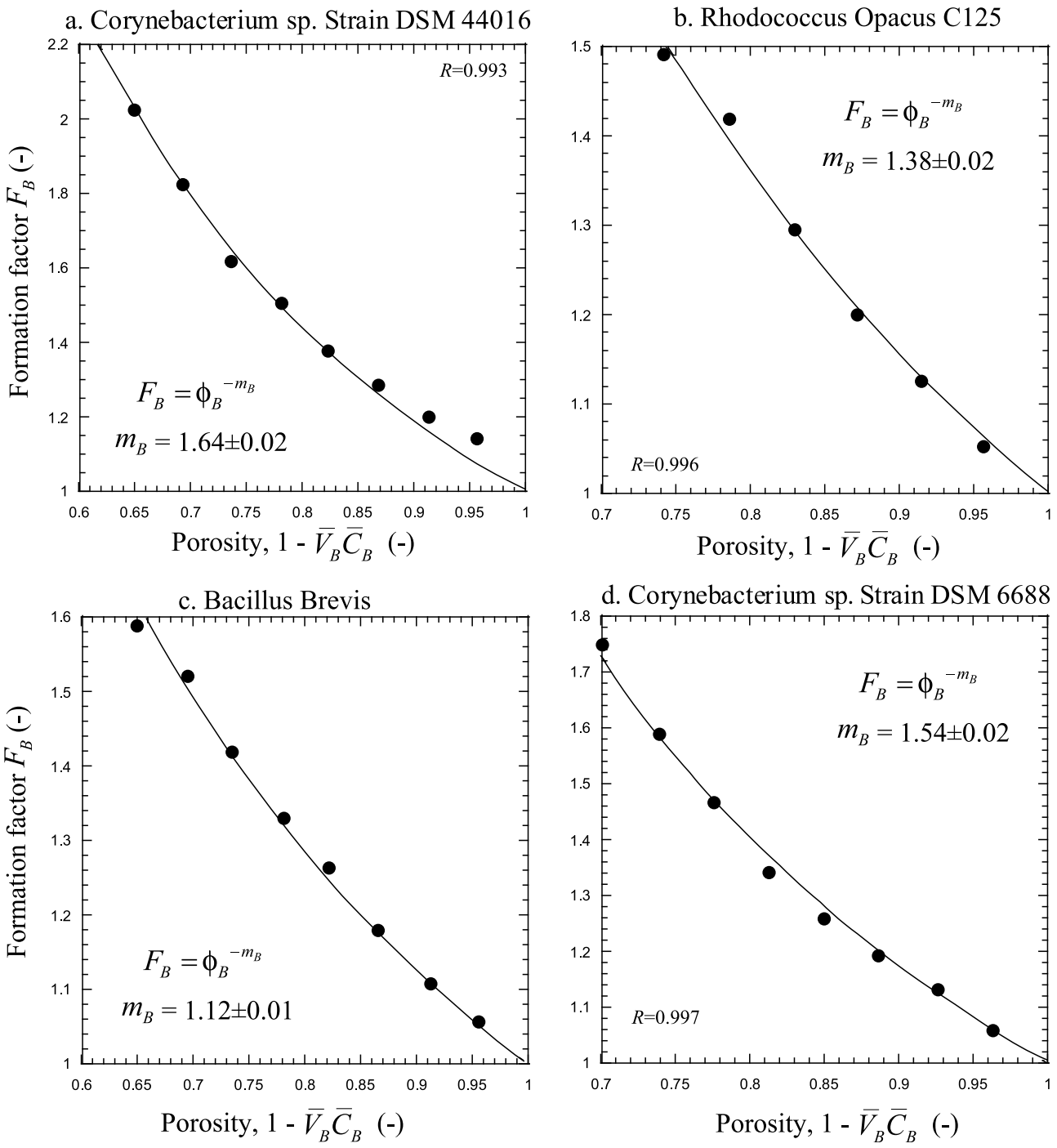

Figure 6. Analysis of the formation factor for a suspension of bacteria. The formation factors are obtained from the analysis done in Figure 5, and the porosity is determined from the concentration of bacteria. The data are fitted by a power law relationship (Archie's law [*Archie*, 1942]) to determine the value of the cementation exponent m_B of the bacteria. For *Rhodococcus erythropolis* A177, $m_B = 1.23 \pm 0.01$ ($R = 0.999$; results not shown here).

(high enough to prevent electrode polarization). This frequency of 3.7 kHz is much higher than the relaxation frequency discussed at the end of section 2. This implies in turn that the measured conductivity is the high-frequency conductivity σ_∞ and not the DC conductivity σ_0.

[38] We first use equation (A3) of Appendix A (Archie's law [*Archie*, 1942]) to determine the value of the formation factor F_B and the surface conductivity $\sigma_S^\infty = \left(m_B\beta_{(+)}\bar{V}_B\rho_B\mathrm{CEC}_B\right)\bar{C}_B$ by fitting the conductivity data versus the pore water conductivity (Figure 6). Then the formation factor is plotted as a function of the porosity (defined as 1 minus the volume fraction of bacteria $\bar{V}_B\bar{C}_B$) and the cementation exponent m_B is determined by fitting Archie's law, which corresponds to a

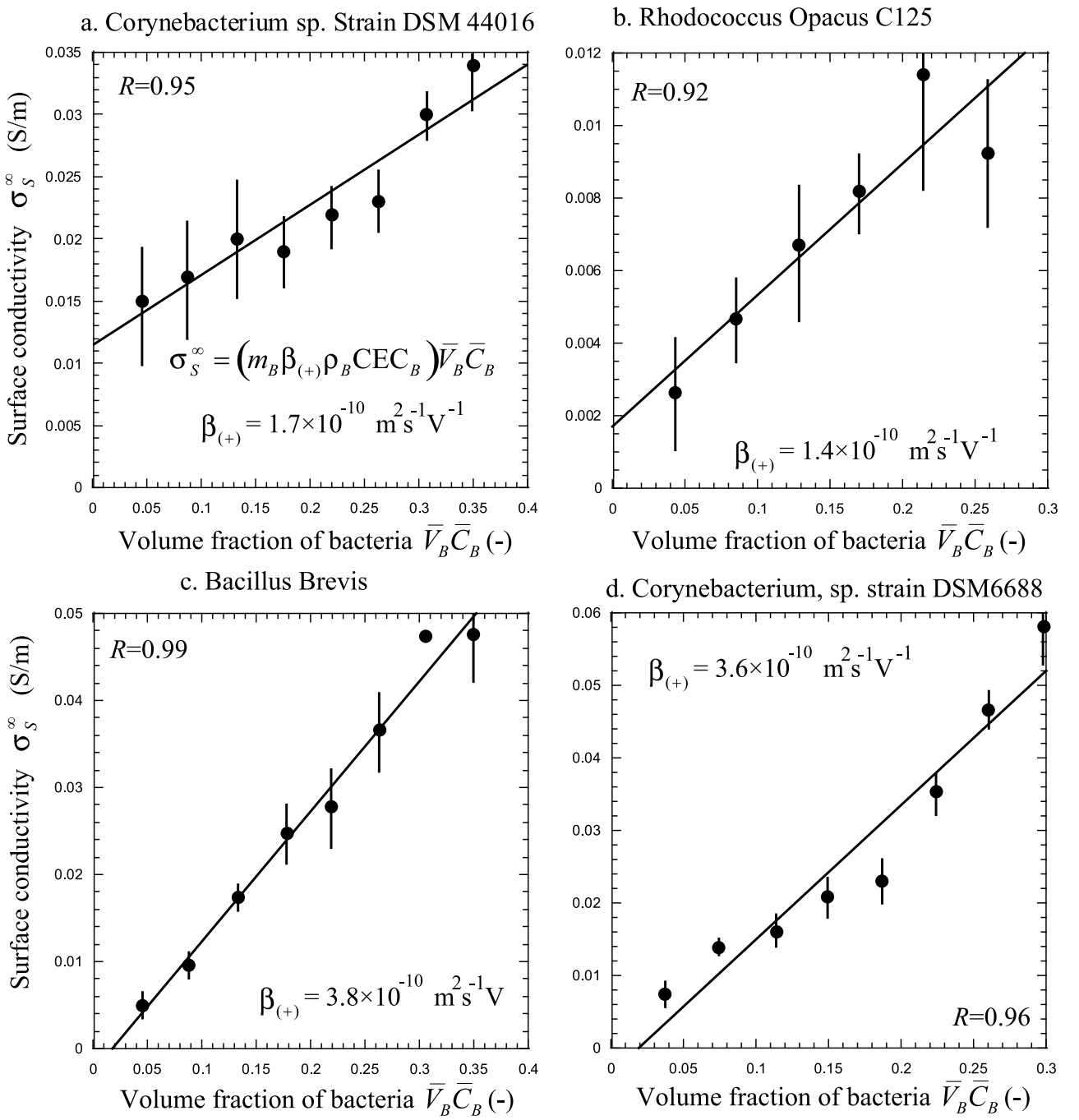

Figure 7. Analysis of the surface conductivity for a suspension of bacteria. The values of the surface conductivity are obtained from the analysis done in Figure 5. The data and the model agree with each other in predicting a linear relationship between these two parameters. The apparent mobility is determined from the slope and the values of the total CEC reported in Table 1. Here pH = 6.5–7.0

power law between the formation factor and the porosity. The cementation exponent is between 1.1 and 1.6, while in theory it should be between 1.5 and 1.7 (see Appendix A for details).

[39] In a second step, we report the surface conductivity σ_S^∞ as a function of the volumetric fraction of bacteria, $\bar{V}_B\bar{C}_B$ (Figure 7) and we determine the apparent mobility of the counterions $\beta_{(+)}$ using $\sigma_S^\infty = \left(m_B\beta_{(+)}\bar{V}_B\rho_B\mathrm{CEC}_B\right)\bar{C}_B$. The value for the mobility of the counterions in the Stern layer of the bacteria is between $\beta_{(+)}(\mathrm{K}^+) \approx 1.7 \times 10^{-10}$ m^2 s^{-1} V^{-1} and 3.8×10^{-10} m^2 s^{-1} V^{-1} at 25°C. This range of values is very close to the mobility of the counterions determined by *Revil* [2012] for clay minerals ($\beta_{(+)}(\mathrm{Na}^+) \approx 1.5 \times 10^{-10}$ m^2 s^{-1} V^{-1}). In Figure 8, we plot the slope of the surface conductivity trends of Figure 7 as a function of the CEC reported in Table 1. From Figure 8, only a fraction of the CEC participate to the surface conductivity. If we wrote the slope of the trends shown in Figure 6 as $b = m_B\beta_{(+)}\rho_B(\delta\mathrm{CEC}_B)$ with $\delta\mathrm{CEC}_B \equiv \mathrm{CEC}_B - \mathrm{CEC}_B^c$ and where CEC_B^c denotes the CEC that does not contribute to surface conductivity, we

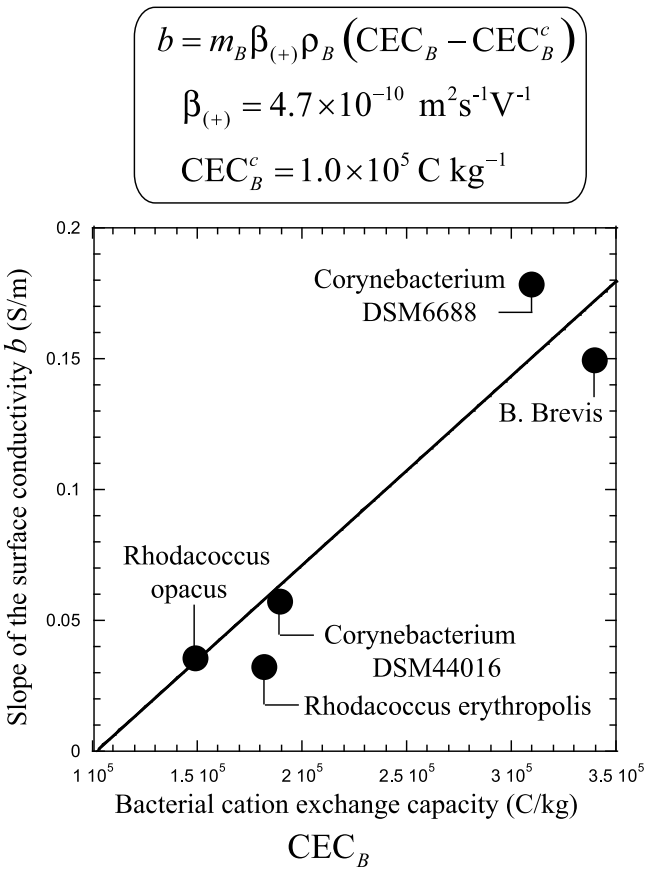

Figure 8. Slope of the surface conductivity trends (determined from Figure 7) as a function of the cation exchange capacity of the individual gram-positive bacteria (from Table 1). Taking m_B = 1.5 and ρ_B = 1020 kg m^{-3} yield a mean value for the mobility of the counterions of $\beta_{(+)} \approx (4.7 \pm 0.8) \times 10^{-10}$ m^2 s^{-1} V^{-1} (R = 0.91). Here pH = 6.5–7.0.

obtain from the trend shown in Figure 7 and using m_B = 1.5 and ρ_B = 1020 kg m^{-3}, $\beta_{(+)} \approx (4.7 \pm 0.8) \times 10^{-10}$ m^2 s^{-1} V^{-1} at 25°C and $\mathrm{CEC}_B^c = 1.0 \times 10^5$ C kg^{-1}.

[40] According to the surface speciation of gram-positive bacteria shown by *Leone et al.* [2007], this behavior is due to the pH dependence of the amino surface groups of the protein and peptidoglycan molecules. Indeed, these sites can accept counterions only at pH > 8. Also the value of the critical CEC determined above can be compared to the CEC from the chemical analysis made by *van der Wal et al.* [1997a] for the contribution of the amino surface groups alone: *Corynebacterium* sp. strain DSM 44016 (0.64 mM g^{-1}), *Corynebacterium* sp. strain DSM 6688 (0.80 mM g^{-1}), *Rhodococcus opacus* C125 (0.56 mM g^{-1}), *Bacillus brevis* (0.96 mM g^{-1}), and *Rhodococcus erythropolis* A177 (0.52 mM g^{-1}).

[41] In gram-negative cells, on the other hand, lipopolysaccharides replace peptidoglycan molecules (Figure 1). Lipopolysaccharides also contain charged phosphate and carboxyl groups but no amino surface groups. Therefore, for gram-negative bacteria, all the CEC may contribute to the surface conductivity and polarization. This will need to be further tested by coupling a triple layer model for different types of bacteria and coupling such triple layer models to electrical properties. Therefore, all the CEC of gram-negative bacteria contribute to surface conductivity and polarization.

[42] The data of *van der Wal et al.* [1997a] exhibit a clear relaxation frequency that they attribute to polarization of the double layer (including a stagnant layer). That said, this polarization takes place well into the kHz range. We disagree therefore with their interpretation of their dispersive data, which is most likely related to Maxwell-Wagner polarization.

3.2. Frequency Dependence of the Conductivity and Permittivity

[43] We use the recent data from *Zhang et al.* [2012] to test the frequency dependence effective electrical properties of a suspensions of *Desulfovibrio vulgaris* (strain Hildenborough/ATCC 35115, a gram-negative bacteria). Impedance spectroscopy was performed with a two-electrode system, which requires a correction of electrode polarization [e.g., *Gråsjö et al.*, 2008]. The data were performed at frequencies from 20 Hz to 1 MHz using two different concentrations of cells (optical density (OD) is used to represent the concentration of cells) of cells. The OD-0.37 suspension corresponds to the higher cell concentration. Measurements were carried out in triplicate and the data shown in Figure 9 were corrected for electrode polarization. The data were fitted using equations (27) and (28) using a Gauss-Newton algorithm. The optimized value of the five model parameters (c, τ, σ_∞, K' and M_n) are reported in Table 3 with their uncertainties. The model fits the data of *Zhang et al.* [2012] very well over the full spectrum of frequencies.

[44] The optimized value of c (0.55 ± 0.05) is close to the theoretical value corresponding to the Warburg impedance model (c = 0.50). The formation factors are determined from the value of the permittivity of Table 3 and equation (30). This yields F_B = 1.9 for OD-0.37 and 1.5 for OD-0.28. This is qualitatively consistent with equation (A4) of Appendix A stating that F_B increases with the bacteria density. Then, we use the values of the formation factors, the optimized values of the normalized chargeabilities reported in Table 3 and equation (26) (time the saturation s_w for a partially saturated sand) to determine the concentration of bacteria. We obtain $\bar{C}_B = 4 \times 10^{14}$ cell m^{-3} for OD-0.37 and $\bar{C}_B = 3 \times 10^{13}$ cell m^{-3} for OD-0.28. Our analysis is therefore qualitatively in agreement with the fact that the suspension characterized by the higher OD corresponds to the higher cell density.

4. Polarization of Bacteria in a Sand

[45] In sections 2 and 3, we have developed and tested a model describing the low-frequency electrical behavior of a suspension of bacteria. In a porous material, the bacteria are expected to be mostly in contact with the solid phase (adhesion). Our goal in this section is to develop a first-order model describing the complex conductivity during the growth of bacteria in a porous material.

4.1. Model

[46] The bacteria are now located in the pore space of the sand (either coating the surface of the grains or in the pore water). The bacteria concentration is now defined as $\bar{C}_B = N_B/V_p$ where N_B is the number of bacteria and V_p the pore volume between the sand grains. A model for the complex conductivity of the porous material with the bacteria located

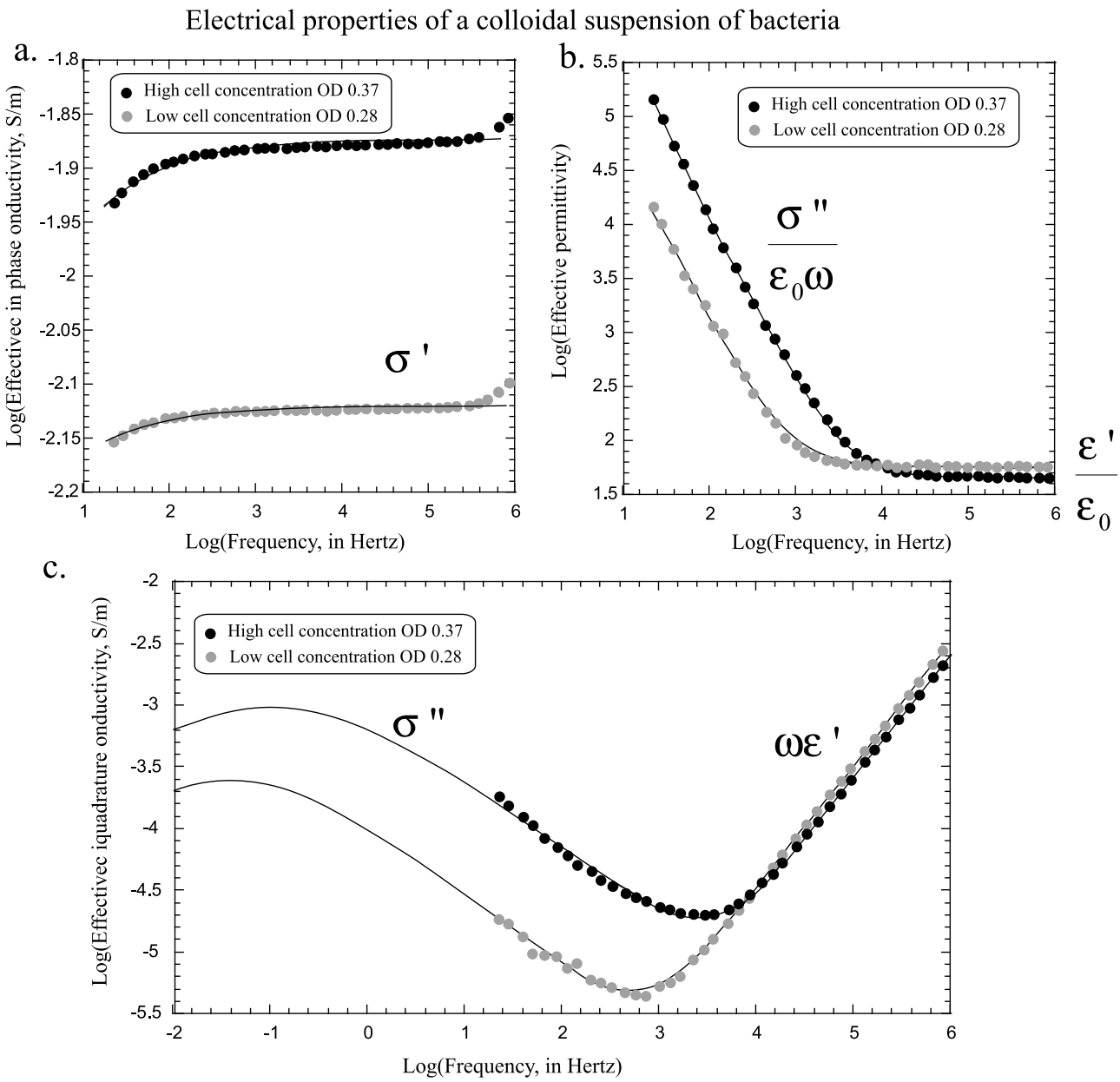

Figure 9. Test of the model for a colloidal suspension of bacteria (*Desulfovibrio vulgaris*, strain Hildenborough/ATCC 35115). Experimental data (circles) from *Zhang et al.* [2012] are in the frequency range 20 Hz to 1 MHz. (a) Effective (in phase or real) conductivity. The asymptotic plateau corresponds to σ_∞. (b) Effective relative permittivity. (c) Magnitude of the effective quadrature conductivity showing the low-frequency α electrical polarization of the cells and the high-frequency dielectric effect. The optimized parameters and their uncertainties are determined by a Gauss-Newton algorithm with the L_2 norm and are reported in Table 3.

in the pore space is given in Appendix B. The maximum of the excess quadrature conductivity of the porous medium containing the bacteria (quadrature conductivity above the background level at the polarization peak) is given by,

$$\sigma''_{B,\max} = -\frac{2}{3}\left(\frac{\phi}{1-\phi}\right)\tan\left[\frac{c\pi}{2}\right]\beta_{(+)}Q_V^B. \quad (33)$$

[47] We can express the charge density in terms of CEC and the quadrature conductivity in terms of the normalized

Table 3. Optimized Parameters for the Data From *Zhang et al.* [2012] Corresponding to a Colloidal Suspension of *Desulfovibrio vulgaris*

Parameters	OD-37	OD-28
Cole-Cole exponent c	0.55 ± 0.05	0.55 ± 0.05
Relaxation time τ (s)	2.6 ± 1.2	2.6 ± 1.2
Conductivity σ_∞ (S m^{-1})	0.0133 ± 0.0002	0.0076 ± 0.0002
Normalized chargeability M_n (S m^{-1})	0.0043 ± 0.0020	0.00047 ± 0.00002
Permittivity K'	45 ± 2	57 ± 3
Chargeability $M = M_n/\sigma_\infty$	0.32	0.06

chargeability. This yields the following expression for the maximum value of the quadrature conductivity or the chargeability:

$$\sigma''_{B,\max} \approx -\tan\left[\frac{c\pi}{2}\right] M_n. \tag{34}$$

$$M_n^B = \frac{2}{3}\left(\frac{\phi}{1-\phi}\right) m_B \left(\beta_{(+)} \bar{V}_B \rho_B \mathrm{CEC}_B\right) \bar{C}_B. \tag{35}$$

[48] We test this model in section 4.2.

4.2. Tests of the Model

[49] To test our model, we used the experimental data of *Davis et al.* [2006]. We choose this data set primarily because the bacterial cells were extracted directly from the soil surfaces. Although cell concentrations can be determined from fluid samples, we note that this underestimates the cell counts and is typically not a true representation of the number of cells present in the pore space of the material because of the high tendency of the bacteria cells to attach to mineral surfaces rather than to live free in the pore water. *Davis et al.* [2006] performed complex conductivity measurements over a broad range of frequencies (0.1–1000 Hz) in two biostimulated sand-packed columns (stimulated columns 1 and 2) and two abiotic control sand columns (control columns 1 and 2). The bacteria present in the biostimulated column include mainly hydrocarbon degraders such as strains of *Variovorax* and *Stenotrophomonas*, (both gram-negative bacteria). Microbial cell concentrations were determined by direct microbial counts on a sampling column experiencing the same conditions as the column in which the induced polarization measurements were performed. Direct count of microbial cell numbers were conducted by direct counting using an epifluorescent microscope [*Bunthof et al.*, 2001] on samples collected from the sampling columns. Bacterial cells were extracted from 0.5 g of wet sand using an extraction technique modified after *Lehman et al.* [2001]. The extracted bacterial cells were washed with 0.85% NaCl solution, stained, and prepared for direct counts using a Live/Dead BacLight Bacterial Viability Kit. The experimental uncertainty was determined by calculating the standard deviation from the average of duplicate counts.

[50] *Davis et al.* [2006] reported that the peak concentration of bacterial cells reached $C_m = 1.2 \times 10^8$ bacteria per gram of wet sand (and not 1.2×10^5 bacteria). *Leone et al.* [2007] reported that there are typically 10^6–10^9 bacteria per gram of soil. The previous concentration can be converted into a cell concentration per unit pore volume of solution $\bar{C}_B$ by

$$\bar{C}_B = C_m \frac{\rho}{s_w \phi}. \tag{36}$$

where s_w denotes the water saturation, $\rho = (1 - \phi)\rho_s + \phi s_w \rho_w + \phi(1 - s_w)\rho_o$ denotes the mass density of the saturated porous sands (ρ_s is the mass density of the solid, 2650 kg m^{-3} for silica, ρ_w and ρ_o correspond to the mass density of water and oil, respectively). Taking $\rho_w = \rho_o = 1000$ kg m^{-3}, we obtain $\rho = 1990$ kg m^{-3}. Taking $s_w = 0.33$ (justified below), the calculation yields a maximum bacteria concentration of 1.8×10^{15} cells m^{-3} (background concentration of 5.4×10^{14} cells m^{-3}). This can be compared to oil-degrading bacteria concentration of 2.4×10^{16} cells m^{-3} in oil-contaminated sands (background concentration of 2 to 9×10^{12} cells m^{-3}) found by *Kostka et al.* [2011] for beach sands contaminated by the Deepwater Horizon oil spill in the Gulf Coast of Mexico.

[51] *Davis et al.* [2006] observed peaks in the quadrature conductivity in the biostimulated columns coincident with peaks in the microbial cell concentrations extracted from the sand in the temporal data. The real conductivity component did not show a relationship to microbial cell concentration. This result can be explained by the low surface conductivity of the sand plus bacteria with respect to the bulk conductivity due to the pore water as discussed below.

[52] In Figure 10, we show the induced polarization spectra at several distinct times during the course of the experiment in one of the control column experiment (column 1) and one of the biostimulated column experiment (column 2). We see that the in-phase conductivity display only a very small change that can be explained by the modest change (a factor 2) in the pore water conductivity (see discussion below). The quadrature conductivity of the stimulated column shows a clear change of its magnitude during the course of the experiment. To isolate the response associated with the bacteria, we use as reference the induced polarization spectrum of the control (unstimulated) column 1 and we performed, at each frequency, the difference between the quadrature conductivity of the column with the bacteria and the quadrature conductivity of the control column. This is justified in Appendix B by the fact that the polarization is associated with the total charge density in the pore space of the sand, which includes the contribution from the grains and the contribution associated with the bacteria.

[53] The type of residual spectrum is shown in Figure 11. It shows clearly a low-frequency α-type polarization with a peak at 2 Hz and a residual dielectric effect above 100 Hz. The nonlinear regression of the data yields the following values of the model parameters: Cole-Cole exponent $c = 0.47 \pm 0.07$, relaxation time $\tau = 0.08 \pm 0.03$ s, and a normalized chargeability $M_n = (3.0 \pm 0.3) \times 10^{-5}$ S m^{-1}. The value of the Cole-Cole exponent is close to the theoretical value corresponding to the Warburg impedance model ($c = 0.5$). The theoretical value of the relaxation time can be determined from equation (32). Using $d_B = 2$ μm [e.g., *de Oliveira-Garcia et al.*, 2002] for *Stenotrophomonas maltophilia*), $\beta_{(+)} = 4.7 \times 10^{-10}$ m^2 s^{-1} V^{-1}, and $T = 25$°C, we obtain $\tau = 0.04$ s (4 Hz) a value close to the inverted value ($\tau = 0.08 \pm 0.03$ s, 2 Hz). Finally, the normalized chargeability can be also inferred from the model. Using $\beta_{(+)} \approx 4.7 \times 10^{-10}$ m^2 s^{-1} V^{-1}, $\phi = 0.40$, $\mathrm{CEC}_B = 2.0 \times 10^5$ C kg^{-1}, $m_B = 1.5$ (see Appendix B), $\bar{V}_B = 1$ μm^3, and $\rho_B = 1020$ kg m^{-3}, we obtain $M_n = 3.8 \times 10^{-5}$ S m^{-1}, a value pretty consistent with the value inverted from the data at the peak of the magnitude of the quadrature conductivity versus time.

[54] During the course of the experiment, the conductivity of the pore water did not change (inside a factor 2) and the value of the pH decreases of 0.5 pH units (Figure 12), which is a minor change regarding its effect on the complexation reactions discussed in section 2. The conductivity of the sand is 0.01 S m^{-1}. The value of the pore water conductivity is in average $\sigma_w = 0.09$ S m^{-1}. At this high pore water

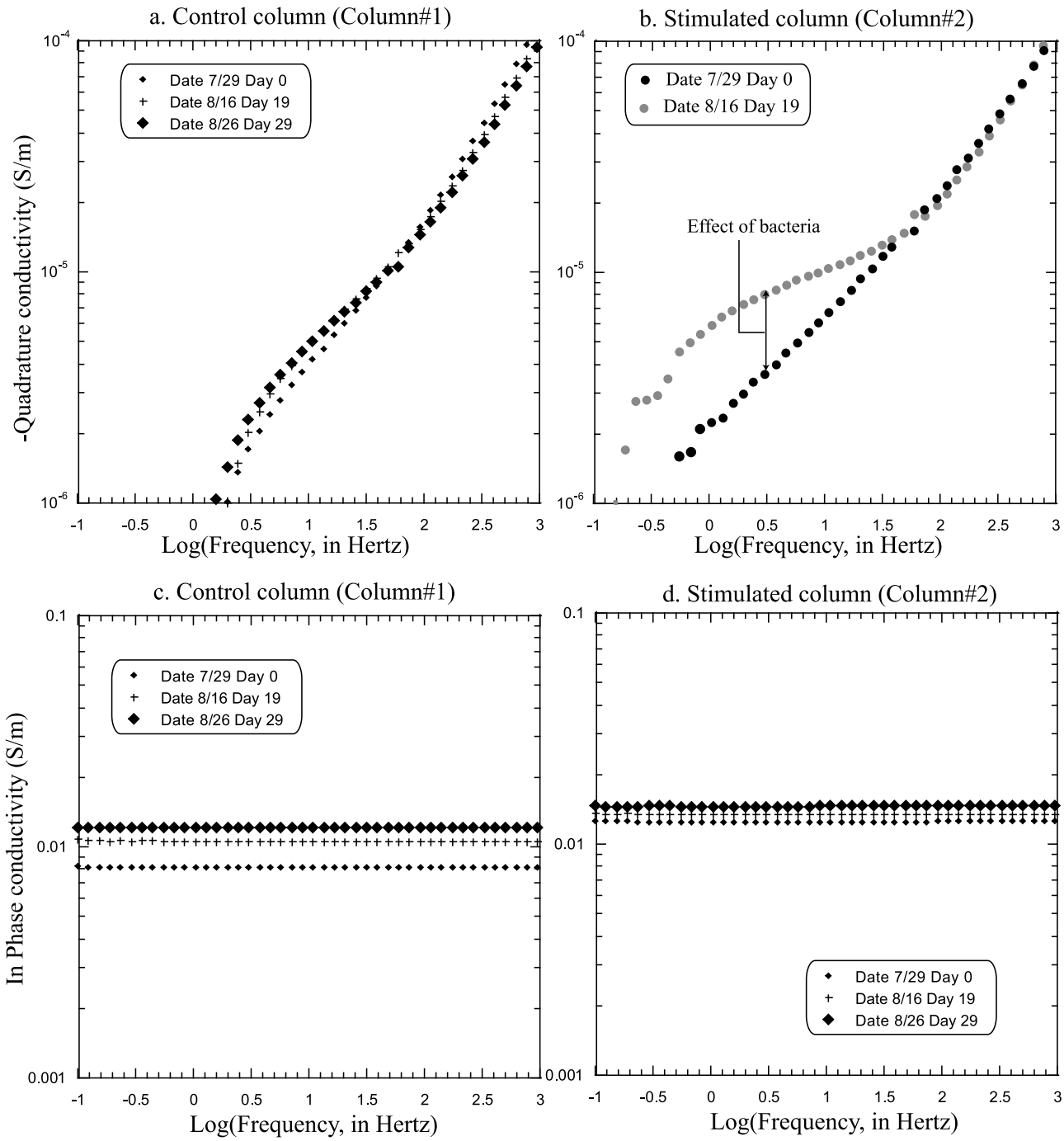

Figure 10. Raw quadrature and in-phase conductivity data for the control and stimulated columns. (a) Quadrature conductivity spectra for control column 1. (b) Same for stimulated column 2. (c) In-phase conductivity for control column 1. (d) Same for the stimulated column. We see that the growth of bacteria is showing up only on the quadrature conductivity.

conductivity, the surface conductivity contribution associated with the sand grains plus bacteria can be neglected. The conductivity of a partially saturated sand is $\sigma = (s_w^2/F)\,\sigma_w$. For well-sorted sands, $F \sim 3$ to 5 with a mean value $\sim$4 [e.g., *Schmutz et al.*, 2010]. Therefore, the saturation in hydrocarbons is estimated to be 67% ($s_w = 0.33$). This should be considered however as a crude estimate. In future modeling efforts, the effect of the change in the water saturation should be accounted for especially if it changes during the course of the experiment. Once the nutrient is exhausted, the saturation should be constant and therefore this saturation effect should not affect the decay part of the curve in Figure 13.

[55] At each time during the course of the experiment, we determine the normalized chargeability. Figure 13a shows the normalized chargeability as a function of time. Using equation (35), we converted these normalized chargeability into bacteria concentrations. The evolution of the bacteria concentration determined from the induced polarization data

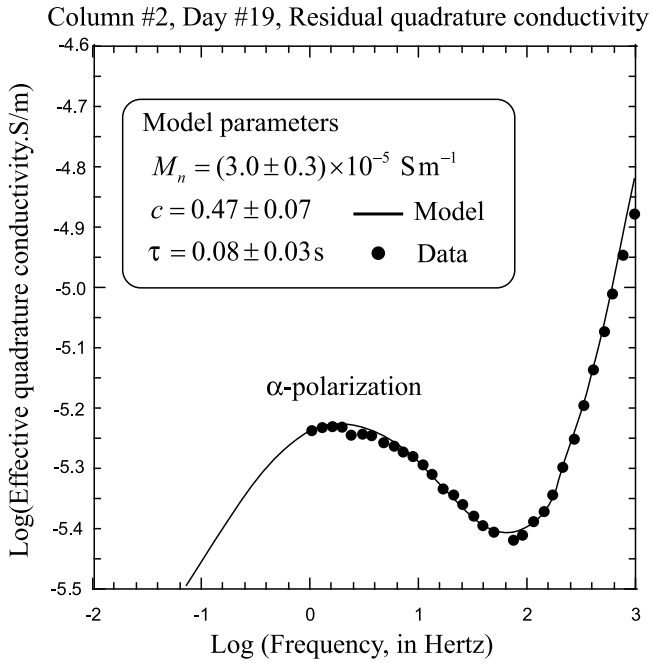

Figure 11. Fit of the magnitude of the residual quadrature conductivity associated with the growth of the bacteria in porous sand for stimulated column 2 (data from *Davis et al.* [2006]). The fit of the model using the expression of the apparent imaginary (quadrature) conductivity $\sigma''_{eff} = \sigma'' + \omega\varepsilon' = \omega\varepsilon_0 K_{eff}$ (R = 0.98). The optimized values of the model parameters are shown on the plot.

is shown in Figure 13b. The results compare fairly well with the few observed values discussed above.

4.3. Endogenous Decay Coefficient From Quadrature Conductivity

[56] The experiment of *Davis et al.* [2006] can be modeled as a batch reactor experiment in which a certain amount of substrate or nutrient S (concentration in mass per volume of pore water) is used by bacteria for their growth. The bacterial growth and the substrate decay can be both modeled by Monod kinetics [*Monod*, 1941, 1949] as follows:

$$\frac{1}{C_B}\frac{dC_B}{dt} = \mu_m\left(1 - \frac{C_B}{K}\right)\left(\frac{S}{K_s + S}\right) - k_d, \tag{37}$$

$$\frac{dS}{dt} = -\frac{1}{Y}\left[\mu_m\left(1 - \frac{C_B}{K}\right)\left(\frac{S}{K_s + S}\right) - k_d\right]C_B, \tag{38}$$

where μ_m is the maximum specific growth rate coefficient (d^{-1}), K is the carrying capacity (units of biomass), K_s is the half saturation constant for that nutrient, i.e., the nutrient concentration at which the specific growth rate is one half the maximum (in mass of nutrient per volume), the yield coefficient Y is used to quantify the yield of organisms per unit substrate consumed; k_d is the first-order rate coefficient for endogenous respiration (endogenous decay coefficient, expressed in s^{-1}). Typical range of values are μ_m = 0.01–2.0 h^{-1}, K_s = 0.1–100 mg L^{-1}, k_d = (5–10) × 10^{-2} d^{-1}. Equations (37) and (38) take into account (1) the growth of bacteria associated with the availability of a substrate, (2) the limitation of the population growth by the capacity of the environment to sustain growth, (3) and the resource-limited growth. In the experiments reported by *Davis et al.* [2006], the initial pore water was a sterile 25% Bushnell Haas (BH) nutrient broth (Becton Dickinson; 50 mg L^{-1} magnesium sulfate, 5 mg L^{-1} calcium chloride, 250 mg L^{-1} monopotassium phosphate, 250 mg L^{-1} diammonium hydrogen phosphate, 250 mg L^{-1} potassium nitrate, 12.5 mg L^{-1} ferric chloride) plus diesel fuel. The biostimulated columns were amended with a mixed bacterial culture containing hydrocarbon degraders such as strains of *Variovorax* (a gram-negative rod-shaped bacteria) and *Stenotrophomonas* (a gram-negative bacillus). That said, the degradation of the substrate was not monitored over time and therefore it is not possible to apply directly equations (37) and (38).

[57] There are typically 7 phases of bacterial growth in a batch reactor experiment considered as a closed system (Figure 14). Phases 2 to 4 correspond to the bacterial growth phase. Phase 7 corresponds to the exponential decay phase (endogenous phase). Phase 7 contains the higher number of measurements in the data given by *Davis et al.* [2006] (see Figures 13a and 15a). In this Phase 7, the substrate has already been exhausted. Setting S = 0 in equation (25), the bacterial decay rate is therefore given by

$$\frac{1}{C_B}\frac{dC_B}{dt} = -k_d, \tag{39}$$

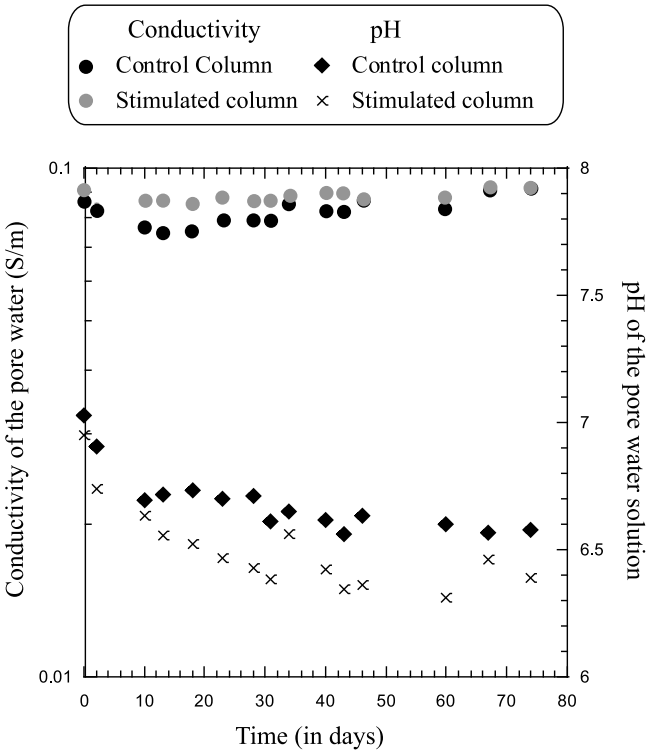

Figure 12. Pore water conductivity and pH versus time for the batch reactor experiment reported by *Davis et al.* [2006]. The solid black symbols represent the unstimulated (reference) column measurements.

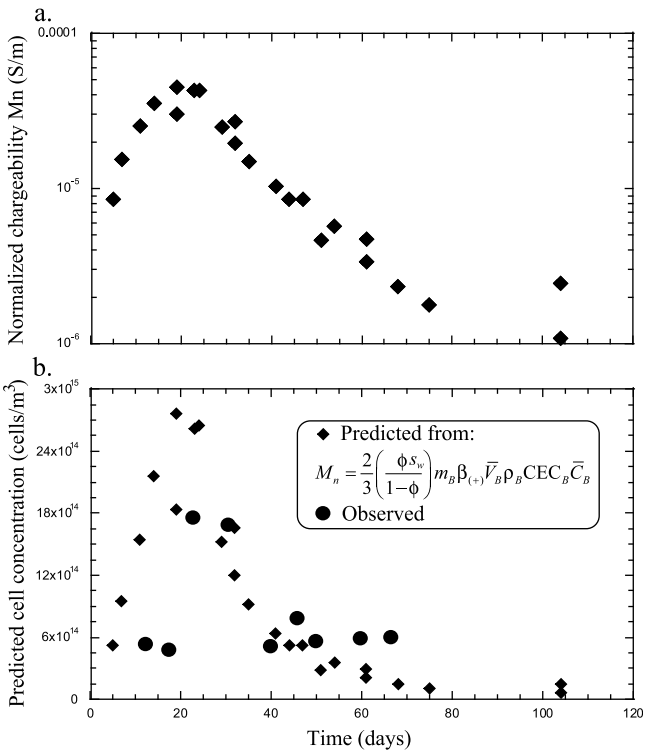

Figure 13. Prediction of the bacteria density (stimulated column 1). We use the optimized values of the normalized chargeability to infer the concentration of the cells in the pore space of the sand. (a) Normalized chargeabilities for the stimulated column. (b) Determination of the number of cells per unit pore volume from the normalized chargeabilities (water saturation s_w = 0.33) and comparison with the observed concentrations.

in this phase. Using the proportionality between the bacterial concentration and the quadrature conductivity, equation (39) can be written as,

$$\frac{1}{\sigma_B''}\frac{d\sigma_B''}{dt} = -k_d. \tag{40}$$

[58] It is important to consider that equation (40) is based only on the second consequence of our model (proportionality between the macroscopic quadrature conductivity and the bacteria density) and does not depend on the value of the mobility of the counterions or the CEC of the bacteria.

[59] Equation (40) can be easily integrated to give the following exponential decay curve

$$\sigma_B''(t) = \sigma_B''(t_0)\exp[-k_d(t-t_0)], \tag{41}$$

where $\sigma_B''(t_0)$ denotes the quadrature conductivity at the beginning of the endogenous phase and t_0 is the time characterizing the beginning of this phase. If we add the background quadrature conductivity value of the sand σ_S'', the total quadrature conductivity is

$$\sigma''(t) = \sigma_B^{M''}\exp[-k_d(t-t_0)] + \sigma_S'', \tag{42}$$

where $\sigma_B^{M''}$ denotes the quadrature conductivity at the beginning of the decay curve (that is the maximum value for the quadrature conductivity curve shown in Figures 15a and 15b. A fit of the data obtained by *Davis et al.* [2006] using equation (42) is shown in Figure 15a. The optimization using a nonlinear least squares fit of the data (with the L_2 norm) yields $\sigma_B^{M''} = (8.8 \pm 0.4) \times 10^{-6}$ S m^{-1}, $k_d = (8.5 \pm 0.8) \times 10^{-2}$ d^{-1}, and $\sigma_S'' = (0.32 \pm 016) \times 10^{-6}$ S m^{-1}. The value of the endogenous decay coefficient k_d is in the range of values reported by *Benefield and Randall* [1980],

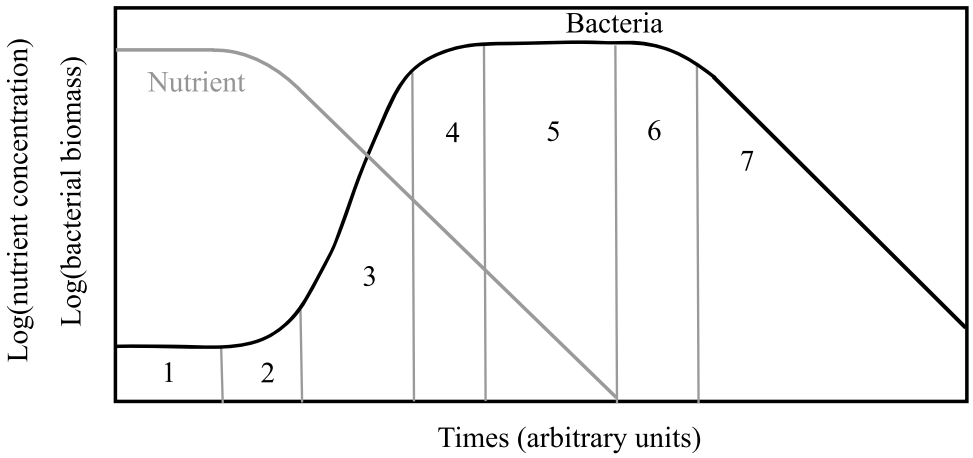

Figure 14. The seven phases of bacterial growth defined by *Buchanan* [1918] for a batch reactor experiment. Phase 1: stationary initial phase needed to convert the substrate in biomass (lag phase). No bacteria growth during this phase. Phase 2: acceleration of the bacterial growing rate (acceleration phase). Phase 3: exponential increase (maximal and constant exponential growth rate; μ_m is given by the slope of the line in this phase). Phase 4: decreasing growth rate due to the gradual decrease in substrate concentration and the increased accumulation of toxic metabolites (the substrate is typically exhausted at the end of this phase). Phase 5: stationary phase (the nutrient is exhausted at the end of this phase, possibly leaving behind a high concentration of toxic metabolites). Phase 6: acceleration of the bacterial decay. Phase 7: exponential decay phase (phase with endogenous metabolism, high death rate, and cell lysis).

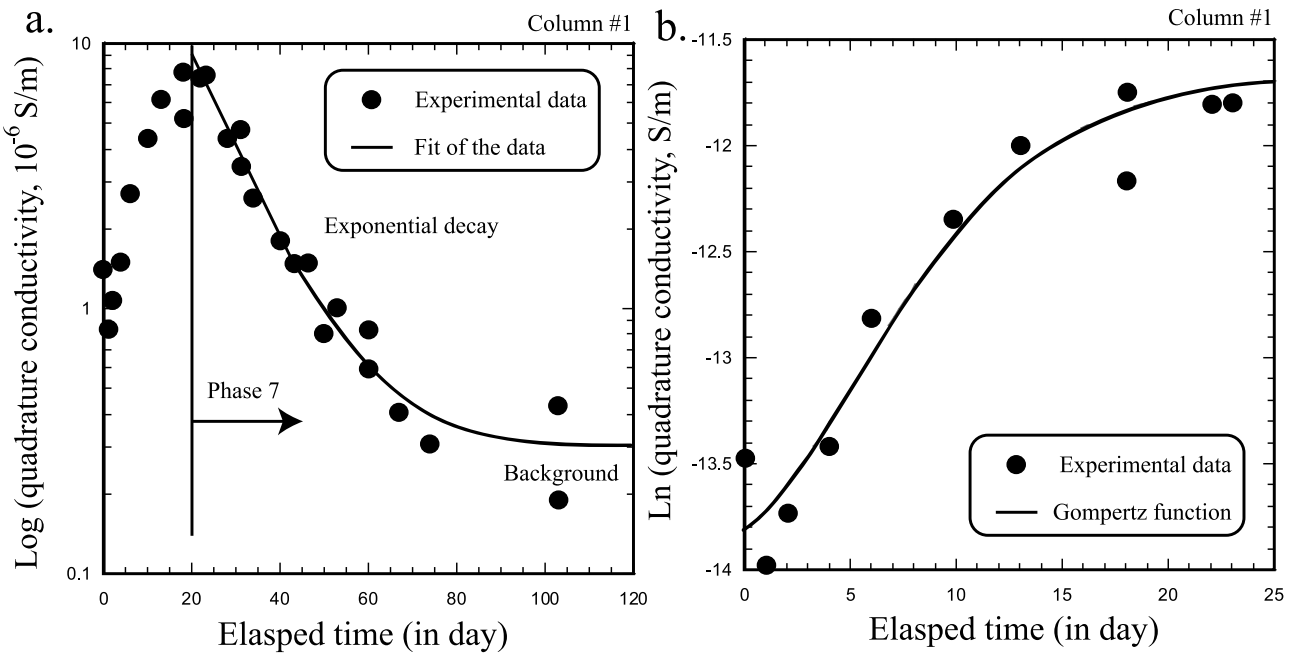

Figure 15. Quadrature conductivity data at 2 Hz for column 1 from *Davis et al.* [2006]. (a) Analysis of the endogenous decay phase (Phase 7 in Figure 14). The line represents the fit of the experimental data of *Davis et al.* [2006] (Phase 7, quadrature conductivity data at 2 Hz, $R = 0.98$) using equation (42). The decay is exponential only at the beginning of Phase 7 before reaching the background value for the quadrature conductivity of the porous material with a residual concentration of bacteria. The optimized model parameters are given in the main text together with their uncertainties. (b) Analysis of the exponential growth phase. The plain line represents the fit of the experimental data of *Davis et al.* [2006] (Phases 2 to 4 in Figure 14; column 1, quadrature conductivity data at 2 Hz, $R = 0.97$) using the Gompertz function, equation (44). The optimized model parameters are given in the main text together with their uncertainties using the least squares approach.

(5 to 10) $\times$ 10^{-2} d^{-1} and similar to the value given by *Ostendorf et al.* [2007] for aerobic biodegradation of petroleum hydrocarbons in unsaturated soils (10.2 $\times$ 10^{-2} d^{-1}). Our estimate of the kinetic parameter k_d has been obtained with no assumption of the value of the CEC of the bacteria.

4.4. Fitting the Initial Bacteria Growth Curve

[60] We investigate now the growth rate with the potential contamination of the induced polarization response by the exhaustion of the nutrient, which is not taken into account in our model. If we assume that the initial bacteria growth is not limited by the availability of the substrate, a simple and broadly used equation to describe the exponential bacteria growth is the Gompertz function [e.g., *Zwietering et al.*, 1990]:

$$C_B(t) = C_B^0 \exp\left\{A \exp\left[-\exp\left[\frac{\mu_m \mathrm{e}}{A}(\tau - t) + 1\right]\right]\right\}, \qquad (43)$$

where $A = \ln(C_B^M/C_B^0)$, C_B^M and C_B^0 denote the maximum and initial values of the bacteria concentrations, respectively, τ is the lag time ($t \ll \tau$ represents the lag defining Phase 1 in Figure 15b), and e = exp(1). We can adapt this function to the quadrature conductivity using the assumption (as done previously) that the change of quadrature conductivity reflects a direct change in bacteria populations and therefore that the change in the nutrient is a second-order effect. This yields

$$\sigma_B''(t) = \sigma_B^{0''} \exp\left\{A \exp\left[-\exp\left[\frac{\mu_m \mathrm{e}}{A}(\tau - t) + 1\right]\right]\right\}, \qquad (44)$$

where $A = \ln(\sigma_B^{M''}/\sigma_B^{0''})$. The data shown in Figures 13 and 15 show that the lag time is very short. Therefore we take $\tau = 0$ in equation (32). We also keep $\sigma_B^{M''} = (8.8 \pm 0.4) \times 10^{-6}$ S m^{-1}. Fitting the Gompertz function, equation (32), to the logarithm of the quadrature conductivity data (see Figure 9) using the least square criteria yields the following values of the two model parameters: $\sigma_B^{0''} = (0.9 \pm 0.1) \times 10^{-6}$ S m^{-1} and $\mu_m = 0.16 \pm 0.02$ d^{-1} (6.7×10^{-3} h^{-1}). It is worth mentioning that the kinetic parameter μ_m has been estimated with no assumption regarding the value of the cation exchange capacity of the bacteria. For aerobic degradation of petroleum hydrocarbons in unsaturated soils, *Ostendorf et al.* [2007] reported μ_m in the range 0.02 to 0.32 d^{-1}. Our value ($\mu_m = 0.16 \pm 0.02$ d^{-1}, Figure 15b) is consistent with this range and values from other literature sources for the biodegradation of diesel (for instance, *Britto et al.* [1996] obtained $\mu_m = 0.11$ d^{-1}).

5. Concluding Statements

[61] The following conclusions have been reached.

[62] 1. We have developed a model connecting directly the density of bacteria in a porous material to its quadrature conductivity (background contribution removed). The surface of the bacteria is highly charged due to the presence of various structures (fibrillar surface protein, capsular polysaccharide, lipopolysaccharide) extending away from the membrane into the pore water solution. The α polarization model we used is based on the migration of the counterions sorbed on the surface of carboxyl, phosphate, and amino groups in this brush of polymeric molecules. This is an important step forward as the evolution of the concentration density of bacteria can be modeled with Monod kinetics and therefore the change of quadrature conductivity can be predicted over time as a function of the environmental variables affecting the growth or decline of bacterial populations.

[63] 2. The quadrature conductivity peaks at quite low frequencies (<10 Hz) because of the very low mobility of the counterions in the Stern layer, which was independently estimated by low-frequency electrical conductivity to be $\beta_{(+)} = 4.7 \times 10^{-10}$ m^2 s^{-1} V^{-1} at 25°C.

[64] 3. The change of the quadrature conductivity with time can be used to determine bacterial growth kinetics parameters like the growth and endogenous decay coefficient k_d, which are derived from the change of the quadrature conductivity with time.

[65] Therefore the present model offers the possibility to use 4D frequency domain induced polarization in the field to monitor biodegradation of oil. These results have implications for microbial enhanced oil recovery and the monitoring of bioremediation of oil spills.

Appendix A: In-phase Conductivity and Permittivity of a Suspension of Bacteria

[66] As shown in *Revil and Florsch* [2010], the conductivity of a suspension of particles can be written as

$$\sigma_\infty = \frac{1}{F_B}(\sigma_w + (F_B - 1)\sigma_B), \tag{A1}$$

where σ_B denotes the conductivity of the bacteria. The bacteria is composed of a membrane encapsulating a cytoplasm. The conductivity of the membrane σ_m is below 10^{-6} S m^{-1} at room temperature [*Asami*, 2002; *Di Biasio and Cametti*, 2011] and is therefore a good insulator. Therefore, the membrane of the bacteria screens off the high conductivity of the interior of the cells (the cytoplasmic conductivity can be pretty high). Consequently, the bacteria appear as insulating particles coated by a conductive electrical double layer and suspended in the background electrolyte. For a suspension of bacteria, the porosity is defined by the fractional volume occupied by the water. Therefore the porosity and the formation factor can be expressed as a function of the volumetric fraction occupied by the bacteria. For a dilute suspension of bacteria,

$$\phi = 1 - \frac{N_B \bar{V}_B}{V} \approx 1 - \bar{C}_B \bar{V}_B, \tag{A2}$$

$$F_B \approx \phi^{-m_B} = (1 - \bar{C}_B \bar{V}_B)^{-m_B}, \tag{A3}$$

$$F_B \approx 1 + m_B \bar{C}_B \bar{V}_B, \tag{A4}$$

$$\frac{1}{F_B} \approx 1 - m_B \bar{C}_B \bar{V}_B, \tag{A5}$$

where V denotes the volume of the colloidal suspension, N_B denotes the number of bacteria, $\bar{V}_B$ their specific volume, and m_B denotes the cementation exponent associated with the shape of the particles (the bacteria in the present case). Equation (A4) is obtained by using a first-order Taylor expansion of equation (A3) and would not be valid for a high density of bacteria. The cementation exponent m_B can be related to the depolarization factor of the particles by [*Sen et al.*, 1981]

$$m_B = \frac{5 - 3L_B}{3\left(1 - L_B^2\right)}. \tag{A6}$$

[67] For prolate spheroids ($a > b = c$, rod shaped), the eccentricity e_B and the depolarization factor L_B are given by

$$e_B = \left(1 - \left(\frac{b}{a}\right)^2\right)^{1/2}, \tag{A7}$$

$$L_B = \frac{1 - e_B}{2{e_B}^3}\left[\ln\left(\frac{1 + e_B}{1 - e_B}\right) - 2e_B\right], \tag{A8}$$

while for oblate spheroids ($a < b = c$), the eccentricity e_B and the depolarization factor L_B are given by

$$e_B = \left(\left(\frac{b}{a}\right)^2 - 1\right)^{1/2}, \tag{A9}$$

$$L_B = \frac{1 + {e_B}^2}{{e_B}^3}\left[e_B - \tan^{-1} e_B\right], \tag{A10}$$

[68] Through these equations, the cementation exponent m_B can be related to the aspect ratio of the bacteria. The cementation exponent is given by $m_B = 1.5$ for spherical bacteria (this value will be taken as a default value in the main text). From equations (A7) and (A8), we obtain $1.5 < m < 1.67$ for rod-shaped bacteria (prolate spheroids).

[69] Using equations (A1) and (A4), we obtain

$$\sigma_\infty = \frac{1}{F_B}(\sigma_w + m_B \bar{C}_B \bar{V}_B \sigma_B). \tag{A11}$$

[70] As explained above, the conductivity of the bacteria is only due to their electrical double layer. Therefore, their conductivity can be related to the cation exchange capacity using

$$\sigma_B = \beta_{(+)} \rho_B \mathrm{CEC}_B. \tag{A12}$$

[71] Combining equations (A11) and (A12) yields in turn the following relationships between the high-frequency electrical conductivity and the concentration of cells or the charge per unit pore volume:

$$\sigma_\infty = \frac{1}{F_B}\left[\sigma_w + \left(m_B \bar{V}_B \beta_{(+)} \rho_B \mathrm{CEC}_B\right)\bar{C}_B\right], \tag{A13}$$

$$\sigma_\infty = \frac{1}{F_B}\left[\sigma_w + m_B \beta_{(+)} Q_V^B\right]. \tag{A14}$$

[72] The high-frequency dielectric constant can be also written with the same composite equation that for the electrical conductivity [*Sen et al.*, 1981]. This yields

$$\varepsilon' = \frac{1}{F}(\varepsilon_w + (F-1)\varepsilon_B). \tag{A15}$$

[73] Note that the cell is a composite of a membrane with the cytoplasm (Figure 4). We note R is the radius of the cell (taken here as a sphere) and d the thickness of the cytoplasm. The dielectric constant of the composite is classically given by the Maxwell formula [e.g., *Asami*, 2002]:

$$\varepsilon_B = \varepsilon_m \frac{2\varepsilon_m + \varepsilon_i - 2\nu(\varepsilon_m - \varepsilon_i)}{2\varepsilon_m + \varepsilon_i + \nu(\varepsilon_m - \varepsilon_i)}, \tag{A16}$$

where $\nu = (1 - d/R)^3$ denotes the volume fraction of the cytoplasm. Note that these equations have been generalized for ellipsoidal cells [e.g., *Di Biasio and Cametti*, 2011] but the equations are pretty difficult to deal with and of no use in the present case. Typically when the thickness of the membrane is very thin (~10 nm), we can take a zero-order approximation of equation (A16) in $(\nu - 1)$ corresponding to $\varepsilon_B \approx \varepsilon_i$.

Appendix B: Quadrature Conductivity of Bacteria in a Porous Material

[74] The quadrature conductivity of a clayey sand is given by [*Revil*, 2012]

$$\sigma''_C = -\frac{2}{3}\left(\frac{\phi}{1-\phi}\right)\beta^S_{(+)}Q^C_V, \tag{B1}$$

where ϕ denotes the porosity of the porous material, $\beta^S_{(+)}$ denotes the mobility of the counterions in the Stern layer, and Q^C_V the volumetric charge density (excess of charge per unit pore volume) due to the clay minerals. There is no effect of the frequency in equation (B1). Indeed, when clays are present, the distribution of the relaxation times is very broad and the quadrature conductivity is observed to be independent on the frequency for a broad ranges of frequencies (~10 mHz to 10 kHz). If we focus on the contribution of the quadrature conductivity associated with the presence of bacteria in the pore space, a simple adaptation of equation (B1) yields

$$\sigma''_B = -\left(\frac{M^B_n}{2}\right)\frac{\cos\left[\frac{\pi}{2}(1-c)\right]}{\cosh[c\ln(\omega\tau)] + \sin\left[\frac{\pi}{2}(1-c)\right]}, \tag{B2}$$

$$M^B_n = \frac{2}{3}\left(\frac{\phi}{1-\phi}\right)m_B\beta_{(+)}Q^B_V, \tag{B3}$$

where M^B_n denotes the normalized chargeability associated with the bacteria and $c = 1/2$ for the Warburg model. We consider $m_B \approx 1.5$ for rod-shaped bacteria. The maximum of the quadrature conductivity is obtained for $\omega = 1/\tau$ and is given by [see *Cole and Cole*, 1941]

$$\sigma''_{B,\mathrm{Max}} = -\left(\frac{M^B_n}{2}\right)\tan\left[\frac{c\pi}{2}\right], \tag{B4}$$

$$\sigma''_{B,\mathrm{Max}} = -\frac{m_B}{3}\left(\frac{\phi}{1-\phi}\right)\tan\left[\frac{c\pi}{2}\right]\beta_{(+)}Q^B_V. \tag{B5}$$

Note that for $c = 0.5$ (Warburg model), $\tan[c\,\pi/2] \approx 0.414$.

[75] **Acknowledgments.** We thank the Office of Science (BER), U.S. Department of Energy (awards DE-FG02-08ER646559 and DE-SC0007118), the NSF (SmartGeo, Project IGERT Intelligent Geosystems; DGE-0801692), and Chevron Energy Technology Company (grant CW852844). We thank L. Slater, J. Munaka Marr, and R. Hort for fruitful discussions and the Associate Editor, M. Hilpert, the Editor, J. Selker, and three referees for helpful suggestions.

References

Abdel Aal, G., E. Atekwana, L. Slater, and E. Atekwana (2004), Effects of microbial processes on electrolytic and interfacial electrical properties of unconsolidated sediments, *Geophys. Res. Lett.*, *31*(12), L12505, doi:10.1029/2004GL020030.

Abdel Aal, G. Z., E. A. Atekwana, S. Rossbach, and D. D. Werkema (2010), Sensitivity of geoelectrical measurements to the presence of bacteria in porous media, *J. Geophys. Res.*, *115*, G03017, doi:10.1029/2009JG001279.

Albrecht, R., J. C. Gourry, M.-O. Simonnot, and C. Leyval (2011), Complex conductivity response to microbial growth and biofilm formation on phenanthrene spiked medium, *J. Appl. Geophys.*, *75*, 558–564, doi:10.1016/j.jappgeo.2011.09.001.

Archie, G. E. (1942), The electrical resistivity log as an aid in determining some reservoir characteristics, *Trans. Am. Inst. Min. Metall. Pet. Eng.*, *146*, 54–62.

Asami, K. (2002), Characterization of biological cells by dielectric spectroscopy, *J. Non. Cryst. Solids*, *305*, 268–277, doi:10.1016/S0022-3093(02)01110-9.

Atekwana, A., and L. Slater (2009), Biogeophysics: A new frontier in Earth science research, *Rev. Geophys.*, *47*, RG4004, doi:10.1029/2009RG000285.

Benefield, L. D., and C. W. Randall (1980), *Biological Process Design for Wastewater Treatment*, Prentice-Hall, Englewood Cliffs, N. J.

Bratbak, G., and I. Dundas (1984), Bacterial dry matter content and biomass estimations, *Appl. Environ. Microbiol.*, *48*(4), 755–757.

Britto, R., J. H. Sherrard, and D. D. Truax (1996), Kinetics of pseudo-continuous flow bioreactor treatment of diesel contaminated soils, *Water Air Soil Pollut.*, *86*, 125–136, doi:10.1007/BF00279150.

Buchanan, R. E. (1918), Life phases in a bacterial culture, *J. Infect. Dis.*, *23*, 109–125.

Bunthof, C. J., S. van Schalkwijk, W. Meijer, T. Abee, and J. Hugenholtz (2001), Fluorescent method for monitoring cheese starter permeabilization and lysis, *Appl. Environ. Microbiol.*, *67*, 4264–4271, doi:10.1128/AEM.67.9.4264-4271.2001.

Cole, K. S., and R. H. Cole (1941), Dispersion and absorption in dielectrics. I. Alternating current characteristics, *J. Chem. Phys.*, *9*, 341–351, doi:10.1063/1.1750906.

Daughney, C. J. and J. B. Fein (1998), The effect of ionic strength on the adsorption of H^+, Cd^{2+}, Pb^{2+}, and Cu^{2+} by *Bacillus subtilis and Bacillus licheniformis*: A surface complexation model, *J. Colloid Interface Sci.*, *198*, 53–77.

Davis, C. A., E. Atekwana, E. Atekwana, L. D. Slater, S. Rossbach, and M. R. Mormile (2006), Microbial growth and biofilm formation in geologic media is detected with complex conductivity measurements, *Geophys. Res. Lett.*, *33*, L18403, doi:10.1029/2006GL027312.

de Oliveira-Garcia, D., M. Dall'Agnol, M. Rosales, A. C. G. S. Azzuz, M. B. Martinez, and J. A. Girón (2002), Characterization of flagella produced by clinical strains of *Stenotrophomonas maltophilia*, *Emerging Infect. Dis.*, *8*(9), 918–923, doi:10.3201/eid0809.010535.

Di Biasio, A., and C. Cametti (2011), On the dielectric relaxation of biological cell suspensions: The effect of the membrane electrical conductivity, *Colloids Surf. B*, *84*, 433–441, doi:10.1016/j.colsurfb.2011.01.038.

Dittrich, M., and S. Sibler (2005), Cell surface groups of two picocyanobacteria strains studied by zeta potential investigations, potentiometric titration, and infrared spectroscopy, *J. Colloid Interface Sci.*, *286*(2), 487–495, doi:10.1016/j.jcis.2005.01.029.

Ferris, L. E., C. L. Davey, and D. B. Kell (1990), Evidence from its temperature dependence that the β-dielectric dispersion of cell suspensions is not due solely to the charging of a static membrane capacitance, *Eur. Biophys. J.*, *18*, 267–276, doi:10.1007/BF00188039.

Gråsjö, J., K. Welch, and M. Strømme (2008), Determining the static dielectric permittivity of ion conducting materials when obscured by electrode polarization, *Appl. Phys. Lett.*, *93*, 092901, doi:10.1063/1.2977861.

Grosse, C. (2002), Relaxation mechanisms of homogeneous particles and cells suspended in aqueous electrolyte solutions, in *Interfacial Electrokinetics and Electrophoresis*, *Surfactant Sci. Ser.*, vol. 106, edited by A. V. Delgado, pp. 277–327, Marcel Dekker, New York.

Hadjoudja, S., V. Deluchat, and M. Baudu (2010), Cell surface characterisation of *Microcystis aeruginosa* and *Chlorella vulgaris*, *J. Colloid Interface Sci.*, *342*, 293–299, doi:10.1016/j.jcis.2009.10.078.

Heinrich, H. T. M., P. J. Bremer, C. J. Daughney, and A. J. McQuillan (2007), Acid–base titrations of functional groups on the surface of the thermophilic bacterium *Anoxybacillus flavithermus*: Comparing a chemical equilibrium model with ATR-IR spectroscopic data, *Langmuir*, *23*, 2731–2740, doi:10.1021/la062401j.

Irimajiri, A., K. Asami, T. Ichinowatari, and Y. Kinoshita (1987), Passive electrical properties of the membrane and cytoplasm of cultured rat basophil leukemia cells. I. Dielectric behavior of cell suspensions in 0.01–500 MHz and its simulation with a single-shell model, *Biochim. Biophys. Acta*, *896*, 203–213, doi:10.1016/0005-2736(87)90181-7.

Karaoulis, M., A. Revil, D. D. Werkema, B. Minsley, W. F. Woodruff, and A. Kemna (2011), Time-lapse 3D inversion of complex conductivity data using an active time constrained (ATC) approach, *Geophys. J. Int.*, *187*, 237–251, doi:10.1111/j.1365-246X.2011.05156.x.

Kostka, J. E., O. Prakash, W. A. Overholt, S. J. Green, G. Freyer, A. Canion, J. Delgardio, N. Norton, T. C. Hazen, and M. Huettel (2011), Hydrocarbon-degrading bacteria and the bacterial community response in Gulf of Mexico beach sands impacted by the Deepwater Horizon oil spill, *Appl. Environ. Microbiol.*, *77*(22), 7962–7974, doi:10.1128/AEM.05402-11.

Lehman, M. R., F. S. Colwell, and G. A. Bala (2001), Attached and unattached microbial communities in a simulated basalt aquifer under fracture- and porous-flow conditions, *Appl. Environ. Microbiol.*, *67*(6), 2799–2809, doi:10.1128/AEM.67.6.2799-2809.2001.

Leone, L., D. Ferri, C. Manfredi, A. Chukarev, S. Sjoberg, and J. Loring (2007), Modeling the acid–base properties of bacterial surfaces: A combined spectroscopic and potentiometric study of the gram-positive bacterium *Bacillus subtilis*, *Environ. Sci. Technol.*, *41*, 6465–6471, doi:10.1021/es070996e.

Leroy, P., and A. Revil (2009), Spectral induced polarization of clays and clay-rocks, *J. Geophys. Res.*, *114*, B10202, doi:10.1029/2008JB006114.

Leroy, P., A. Revil, A. Kemna, P. Cosenza, and A. Gorbani (2008), Spectral induced polarization of water-saturated packs of glass beads, *J. Colloid Interface Sci.*, *321*(1), 103–117, doi:10.1016/j.jcis.2007.12.031.

Monod, J. (1941), Croissance des populations bactériennes en fonction de la concentration de l'aliment hydrocarbonné, *C. R. Hebd. Seances Acad. Sci.*, *212*, 771–773.

Monod, J. (1949), The growth of bacterial cultures, *Annu. Rev. Microbiol.*, *3*, 371–394, doi:10.1146/annurev.mi.03.100149.002103.

Ntarlagiannis, D., N. Yee, and L. Slater (2005a), On the low-frequency electrical polarization of bacterial cells in sands, *Geophys. Res. Lett.*, *32*, L24402, doi:10.1029/2005GL024751.

Ntarlagiannis, D., K. H. Williams, L. Slater, and S. Hubbard (2005b), The low frequency response to microbial induced sulfide precipitation, *J. Geophys. Res.*, *110*, G02009, doi:10.1029/2005JG000024.

Ohshima, H. (2002), *Encyclopedia of Surface and Colloid Science*, pp. 1834–1852, Marcel Dekker, New York.

Ostendorf, D. W., T. H. Schoenberg, E. S. Hinlein, and S. C. Long (2007), Monod kinetics for aerobic biodegradation of petroleum hydrocarbons in unsaturated soil microcosms, *Environ. Sci. Technol.*, *41*(7), 2343–2349, doi:10.1021/es062313l.

Personna, Y. R., D. Ntarlagiannis, L. Slater, N. Yee, M. O'Brien, and S. Hubbard (2008), Spectral induced polarization and electrodic potential monitoring of microbially mediated iron sulfide transformations, *J. Geophys. Res.*, *113*, G02020, doi:10.1029/2007JG000614.

Poortinga, A. T., R. Bos, W. Norde, and H. J. Busscher (2002), Electrical double layer interactions in bacterial adhesion to surfaces, *Surf. Sci. Rep.*, *47*, 1–32, doi:10.1016/S0167-5729(02)00032-8.

Revil, A. (2012), Spectral induced polarization of shaly sands: Influence of the electrical double layer, *Water Resour. Res.*, *48*, W02517, doi:10.1029/2011WR011260.

Revil, A., and N. Florsch (2010), Determination of permeability from spectral induced polarization in granular media, *Geophys. J. Int.*, *181*, 1480–1498, doi:10.1111/j.1365-246X.2010.04573.x.

Revil, A., C. A. Mendonça, E. Atekwana, B. Kulessa, S. S. Hubbard, and K. Bolhen (2010), Understanding biogeobatteries: Where geophysics meets microbiology, *J. Geophys. Res.*, *115*, G00G02, doi:10.1029/2009JG001065.

Schmutz, M., A. Revil, P. Vaudelet, M. Batzle, P. Femenía Viñao, and D. D. Werkema (2010), Influence of oil saturation upon spectral induced polarization of oil bearing sands, *Geophys. J. Int.*, *183*, 211–224, doi:10.1111/j.1365-246X.2010.04751.x.

Schwarz, G. (1962), A theory of the low-frequency dielectric dispersion of colloidal particles in electrolyte solution, *J. Phys. Chem.*, *66*, 2636–2642, doi:10.1021/j100818a067.

Sen, P. N., C. Scala, and M. H. Cohen (1981), Self-similar model for sedimentary rocks with application to the dielectric constant of fused glass beads, *Geophysics*, *46*, 781–795.

Siano, S. A. (1997), Biomass measurement by inductive permittivity, *Biotechnol. Bioeng.*, *55*, 289–304, doi:10.1002/(SICI)1097-0290(19970720)55:2<289::AID-BIT7>3.0.CO;2-E.

Slater, L., D. Ntarlagiannis, Y. R. Personna, and S. Hubbard (2007), Pore-scale spectral induced polarization signatures associated with FeS biomineral transformations, *Geophys. Res. Lett.*, *34*, L21404, doi:10.1029/2007GL031840.

van der Wal, A., M. Minor, W. Norde, A. J. B. Zehnder, and J. Lyklema (1997a), Electrokinetic potential of bacterial cells, *Langmuir*, *13*, 165–171, doi:10.1021/la960386k.

van der Wal, A., M. Minor, W. Norde, A. J. B. Zehnder, and J. Lyklema (1997b), Conductivity and dielectric dispersion of gram-positive bacteria cells, *J. Colloid Interface Sci.*, *186*, 71–79.

Vaudelet, P., A. Revil, M. Schmutz, M. Franceschi, and P. Bégassat (2011a), Induced polarization signature of the presence of copper in saturated sands, *Water Resour. Res.*, *47*, W02526, doi:10.1029/2010WR009310.

Vaudelet, P., A. Revil, M. Schmutz, M. Franceschi, and P. Bégassat (2011b), Changes in induced polarization associated with the sorption of sodium, lead, and zinc on silica sands, *J. Colloid Interface Sci.*, *360*, 739–752, doi:10.1016/j.jcis.2011.04.077.

Vinegar, H. J., and M. H. Waxman (1984), Induced polarization of shaly sands, *Geophysics*, *49*, 1267–1287.

Walker, S. L., J. E. Hill, J. A. Redman, and M. Elimelech (2005), Influence of growth phase on adhesion kinetics of *Escherichia coli* D21g, *Appl. Environ. Microbiol.*, *71*(6), 3093–3099, doi:10.1128/AEM.71.6.3093-3099.2005.

Warburg, E. (1899), Über das Verhalten sogenannter unpolarisiebarer Elektroden gegen Wechelstrom, *Ann. Phys. Chem*, *67*, 493–499.

Williams, K. H., D. Ntarlagiannis, L. D. Slater, A. Dohnalkova, S. S. Hubbard, and J. F. Banfield (2005), Geophysical imaging of stimulated microbial biomineralization, *Environ. Sci. Technol.*, *39*(19), 7592–7600, doi:10.1021/es0504035.

Williams, K. H., A. Kemna, M. Wilkins, J. Druhan, E. Arntzen, A. L. N'Guessan, P. E. Long, S. S. Hubbard, and J. F. Banfield (2009), Geophysical monitoring of coupled microbial and geochemical processes during stimulated subsurface bioremediation, *Environ. Sci. Technol.*, *43*(17), 6717–6723, doi:10.1021/es900855j.

Wong, J. (1979), An electrochemical model of the induced-polarization phenomenon in disseminated sulfide ores, *Geophysics*, *44*(7), 1245–1265, doi:10.1190/1.1441005.

Zhang, C., L. Slater, and C. Prodan (2012), Complex dielectric properties of sulfate-reducing bacteria suspensions, *Geomicrobiol. J.*, in press.

Zwietering, M. H., I. Jongenburger, F. M. Rombouts, and K. van'T Riet (1990), Modeling of the bacterial growth curve, *Appl. Environ. Microbiol.*, *55*, 1875–1881.